

Ultra High Energy Neutrinos: Absorption, Thermal Effects and Signatures

Cecilia Lunardini, Eray Sabancilar, Lili Yang

Physics Department, Arizona State University, Tempe, Arizona 85287, USA.

E-mail: Cecilia.Lunardini@asu.edu, Eray.Sabancilar@asu.edu, lyang54@asu.edu

Abstract. We study absorption of ultra high energy neutrinos by the cosmic neutrino background, with full inclusion of the effect of the thermal distribution of the background on the resonant annihilation channel. For a hierarchical neutrino mass spectrum (with at least one neutrino with mass below $\sim 10^{-2}$ eV), thermal effects are important for ultra high energy neutrino sources at $z \gtrsim 16$. The neutrino transmission probability shows no more than two separate suppression dips since the two lightest mass eigenstates contribute as a single species when thermal effects are included. Results are applied to a number of models of ultra high energy neutrino emission. Suppression effects are strong for sources that extend beyond $z \sim 10$, which can be realized for certain top down scenarios, such as superheavy dark matter decays, cosmic strings and cosmic necklaces. For these, a broad suppression valley should affect the neutrino spectrum at least in the energy interval $10^{12} - 10^{13}$ GeV – which therefore is disfavored for ultra high energy neutrino searches – with only a mild dependence on the neutrino mass spectrum and hierarchy. The observation of absorption effects would indicate a population of sources beyond $z \sim 10$, and favor top-down mechanisms; it would also be an interesting probe of the physics of the relic neutrino background in the unexplored redshift interval $z \sim 10 - 100$.

Contents

1	Introduction	1
2	Generalities	3
2.1	Searching for UHE neutrinos: limits and sensitivity	3
2.2	Neutrino masses and mixing	4
2.3	Cosmic neutrino background	6
3	Neutrino absorption effects	7
3.1	Cross sections	8
3.2	Optical depth and flux suppression	11
4	Ultra high energy neutrino flux	12
4.1	Top down neutrino sources	13
4.1.1	Cosmic strings	15
4.1.2	Cosmic necklaces	16
4.1.3	Superheavy dark matter	17
4.2	Astrophysical neutrino sources	17
4.2.1	Cosmogenic neutrinos	17
4.3	Gamma ray bursts and active galactic nuclei	19
5	Discussion	20
A	Cross sections	22
A.1	Resonant cross section	22
A.2	Non-resonant cross sections	23
B	Scattering amplitude and rate	24

1 Introduction

It is remarkable how our knowledge of the neutrino sky has so far been limited to a narrow band, from keV to a few TeV of energy, only recently reaching the PeV scale [1]. Extending this range, in both directions, will reveal new phenomena, some of completely unknown nature so far. The high energy frontier is expected to be especially rich, with neutrinos from baryonic accelerators (gamma ray bursts, active galactic nuclei, etc.), extending up to about 10^9 GeV or so. At even higher energy, the ultra high energy (UHE) regime will show cosmogenic neutrinos, and may even reveal the existence of topological defects, which could emit neutrinos through a number of energy loss channels. For those sources far beyond the gamma ray horizon (redshift $z \sim 0.1$ for 1 TeV energy [2]) neutrinos might very well be the only probe, since, even at the highest energies, they propagate freely up to cosmological distances [3].

At this time, experiments dedicated to the UHE regime are advancing rapidly: after a first successful phase, a new generation of experiments is expected to come online, and start to probe the parameter space predicted by theory. The prospects of a detection of UHE

neutrinos is of great motivation to model the expected fluxes in detail, including a number of propagation effects like flavor oscillations and absorption, and possible other phenomena due to still unknown neutrino properties, like neutrino decay or non-standard interactions. Neutrino absorption is the focus of the present work.

Absorption of UHE neutrinos is largely due to scattering on the cosmic neutrino background (C ν B), and, for energies $E \gtrsim 10^{11}$ GeV, it establishes a neutrino “horizon” of $z \sim 140$, beyond which the Universe is opaque to neutrinos [3]. In fact, the shape of this horizon is rather complicated, because the neutrino mean free path is resonantly suppressed – depending on the neutrino energy and mass – due to neutrino-antineutrino annihilation via the Z^0 boson ($\nu + \bar{\nu} \rightarrow$ anything). The signature of this process is one or more characteristic absorption dips in the neutrino spectrum.

The phenomenology of resonant absorption has been studied in various contexts, starting with the so called “Z-burst” scenario [4, 5], to explain possible cosmic ray events beyond the Greisen Zatsepin Kuzmin (GZK) cutoff of cosmic rays [6, 7]. Subsequent works focused on modeling the sharp dips expected for non-relativistic neutrino background [8, 9]. It was then considered that, at least for the lowest of the three neutrino masses, thermal effects on the C ν B might be important. These were studied in detail for a single neutrino species [10], and the transmission probabilities were calculated in the context of a more realistic three-neutrino mass spectrum [11].

The time is now mature to continue the study of this topic in a fully realistic way, with a stronger attention to applications to realistic models of UHE neutrino sources. To include all suppression effects is especially important, to estimate the level of sensitivity required for detection, and to correctly interpret future observations. Considering our improving knowledge of the neutrino mixing matrix, and the expectation that the neutrino masses may be measured soon in the laboratory, it is likely that absorption signatures in UHE neutrino data will be used effectively as probes of the physics of the sources and of the C ν B. Specifically, a strong (weak) suppression would favor a population of sources at distance comparable to (smaller than) the neutrino horizon. The degree of suppression could also provide a direct detection of the C ν B, and probe, at least in principle, its density, momentum distribution and possible exotic properties.

Here we develop a fully realistic treatment of the absorption: considering the three active neutrino species, we include thermal effects exactly (Fig. 1), and discuss their dependence on the neutrino mass spectrum. The results are applied to a number of proposed mechanisms of production of UHE neutrinos, including astrophysical sources, massive relics and topological defects. The goal is to identify the main signatures at near future experiments, and discuss what physics can be learned from them.

The paper is organized as follows. In Sec. 2, we give generalities on the detectability of UHE neutrinos, and discuss the physics of neutrinos and of the C ν B. In Sec. 3, absorption effects are discussed, with emphasis on thermal effects. In Sec. 4, we consider a number of UHE neutrino sources, and for each of them, we discuss the signatures of neutrino absorption on the expected signal at Earth. The results are then discussed in Sec. 5. Appendix A summarizes the details of the calculation of the relevant neutrino cross sections (resonant and non-resonant). In Appendix B, we elaborate on the effect of neutrino mixing on the scattering rate.

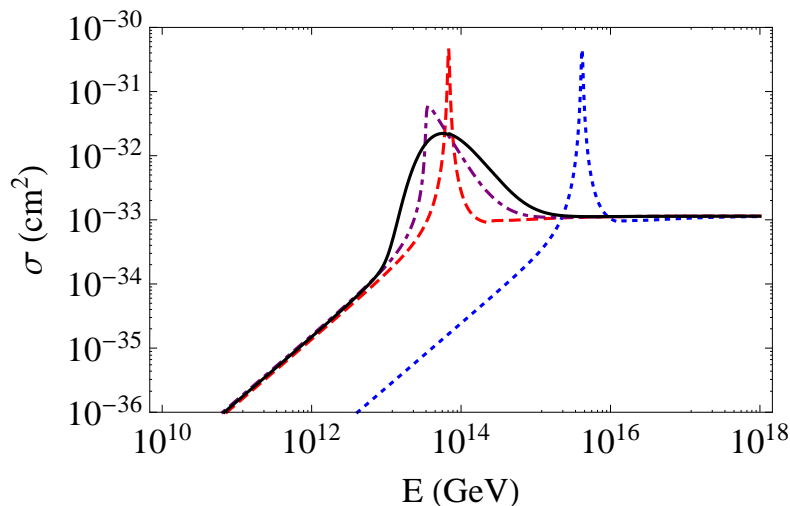


Figure 1. The total ($\nu + \bar{\nu} \rightarrow \text{anything}$) cross section, as a function of the beam energy, for a thermal neutrino background of temperature $T = 1.714 \times 10^{-2}$ eV (corresponding to redshift $z = 100$) and a background neutrino of mass $m = 10^{-3}$ eV. The curves correspond to different levels of inclusion of thermal effects: (i) Dotted (blue): no thermal effects (target neutrino at rest), (ii) Dashed (red): same as (i), but with an effective value of the center of mass energy [see Eq. (3.5)], (iii) Dot-dashed (purple): for background neutrino momentum fixed at its root mean square value and averaged over the scattering angle, (iv) Solid (black): full calculation (this work), after averaging over the background momentum distribution and scattering angle (see Sec. 3).

2 Generalities

2.1 Searching for UHE neutrinos: limits and sensitivity

UHE neutrinos of energies $E \gtrsim 10^{10}$ GeV are very interesting as a testing ground for several high energy astrophysical mechanisms and top down models, as well as of new neutrino detection methods. The space mission JEM-EUSO [30–32] will use Earth’s atmosphere as the target medium to detect fluorescent light from extensive air showers, and will be most sensitive at energies $E \sim 10^{10} - 10^{11}$ GeV. Another efficient UHE neutrino detection method is the so called radio Cherenkov technique that is based on the Askaryan effect [12]. This effect was successfully tested and observed in a lab experiment [13] and in Antarctic ice [14]. Specific implementations of this technique have used the lunar regolith as target medium (GLUE [15], NuMoon [16–18] and RESUN [19]) or the ice of Greenland (FORTE [20]) or the polar cap in Antarctica (ANITA [21–23] and RICE [24]). A new generation of ongoing or planned initiatives will bring this method to its full potential. The main projects are LOFAR [25–27], SKA [28, 29], LUNASKA [33, 34], ARIANNA [35], AURA [36, 37] and EVA [38].

In Fig. 2, we show the expected sensitivities from LOFAR, SKA and JEM-EUSO as well as the upper bounds on the UHE neutrino flux from RICE, ANITA, FORTE and NuMoon. The figure also shows some expected UHE neutrino fluxes from various sources, such as cosmogenic neutrinos, active galactic nuclei, superheavy dark matter decays, cosmic string cusps and kinks, superconducting cosmic strings and cosmic necklaces. We shall elaborate in detail on these in Sec. 4.

All the UHE neutrinos fluxes we consider here originate from hadronic cascades that produce numerous pions, which eventually decay into neutrinos, electrons, positrons and

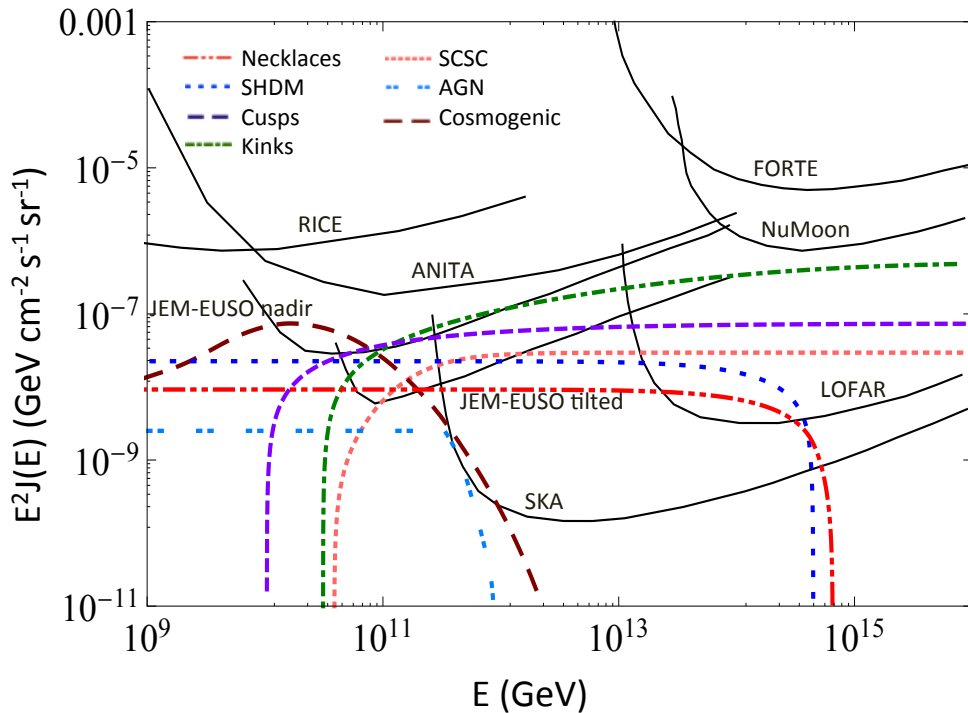


Figure 2. Solid (black) curves: existing upper bounds on the UHE neutrino flux from RICE, ANITA, FORTE, NuMoon, and expected sensitivities at JEM-EUSO (nadir and tilted modes), LOFAR and SKA. Non-solid (color) curves: UHE neutrino fluxes from cosmic string cusps, cosmic string kinks, superconducting cosmic string cusps (SCSC), cosmic necklaces, superheavy dark matter (SHDM), cosmogenic neutrinos and active galactic nuclei (AGN) (see the legend in the figure).

photons. About half the initial energy density in pions goes to electromagnetic energy density including high energy e^\pm and γ -rays. These particles have very short mean free paths since they interact electromagnetically with the background photons (CMB and extragalactic background light). The initial electromagnetic energy density quickly cascades down to lower energy photons leaving a diffuse flux of γ -ray photons behind. Therefore, one can obtain an upper bound on UHE neutrino flux based on the observed diffuse γ -ray background, as was first considered by Berezhinsky and Smirnov [39]. The most recent upper limit is based on the Fermi-LAT observations [40] of the γ -rays [41]. We checked that the example fluxes shown in Fig. 2 are consistent with this cascade upper bound.

2.2 Neutrino masses and mixing

For decades after its discovery, the neutrino has remained a mysterious particle in its fundamental properties. The question if neutrinos are massive or not has remained open for decades, during which laboratory limits have narrowed down the neutrino mass to a few eV [42, 43]. This scale has been recently surpassed (although in a parameter-dependent way) by cosmological probes yielding upper limits on the sum of the neutrino masses. At 95% CL, the main limits are $\Sigma m_\nu < 0.44$ eV by the WMAP 9-year data [44] and $\Sigma m_\nu < 0.23$ eV by the recent Planck data [45].

The fact that neutrinos have mass has finally been established through the discovery of neutrino flavor oscillations. Indeed, in the absence of exotic neutrino interactions, oscillations

are possible only if there are two physically distinct bases for a system of three neutrinos: the basis of the mass eigenstates, ν_i (with masses m_i , $i = 1, 2, 3$), and the basis of eigenstates of the weak interaction (flavor states), ν_α with $\alpha = e, \mu, \tau$. Oscillation probabilities depend on the mixing matrix connecting the two bases, and on the mass squared differences $\Delta m_{ij}^2 \equiv m_i^2 - m_j^2$. The latter are measured to be $\Delta m_{21}^2 \simeq 7.5 \times 10^{-5} \text{ eV}^2$ and $|\Delta m_{31}^2| \simeq 2.4 \times 10^{-3} \text{ eV}^2$ (see e.g., [46]), indicating that:

1. There are two possibilities, or *hierarchies*: $m_1 < m_2 < m_3$ (normal hierarchy, NH) and $m_3 < m_1 < m_2$ (inverted hierarchy, IH).
2. At least two of the three masses are not zero: for NH, we have $m_2 \gtrsim 8.6 \times 10^{-3} \text{ eV}$ and $m_3 \gtrsim 4.8 \times 10^{-2} \text{ eV}$; for IH we get $m_1 \sim m_2 \gtrsim 4.8 \times 10^{-2} \text{ eV}$. Fig. 3 illustrates the possible values of the three masses depending on the hierarchy. We distinguish between a *hierarchical* mass spectrum, where at least two of the masses differ by one or more orders of magnitude, and a *degenerate* spectrum with masses of comparable value. As the figure shows, the degenerate case requires the smallest mass ($m_{\min} = m_1$ or m_3 depending on the hierarchy) to exceed a few times 10^{-2} eV .

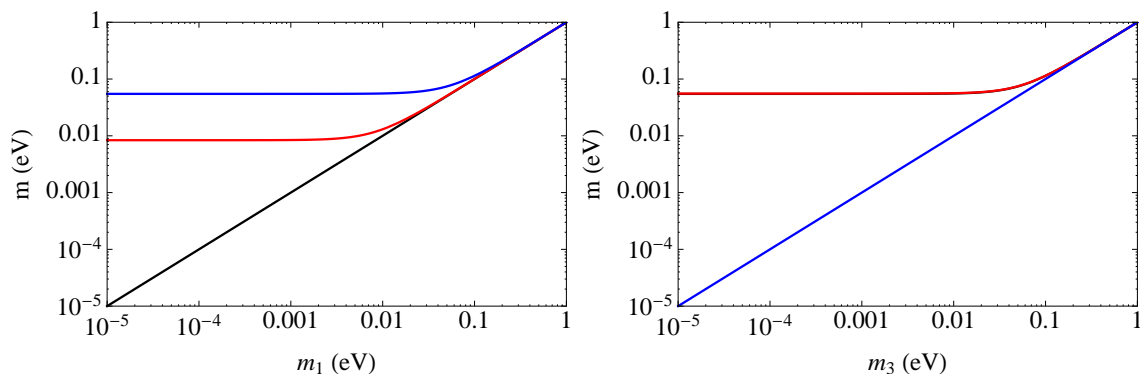


Figure 3. The three neutrino masses as a function of the minimum mass m_{\min} . The left (right) panel is for the normal (inverted) hierarchy, where $m_{\min} = m_1$ ($m_{\min} = m_3$).

Here we choose to work with eight representative mass spectra (see Table 1), four for each hierarchy, where the smallest mass equals $m_{\min} = 10^{-5}, 10^{-3}, 2 \times 10^{-2}, 8 \times 10^{-2} \text{ eV}$. In order, these correspond to spectra that are extremely hierarchical, moderately hierarchical, moderately degenerate and very degenerate.

m_1	m_2	m_3	m_1	m_2	m_3
0.00001	0.0084	0.055	0.055	0.055	0.00001
0.001	0.0084	0.055	0.055	0.055	0.001
0.02	0.022	0.058	0.058	0.059	0.02
0.08	0.080	0.097	0.097	0.097	0.08

Table 1. Values of the neutrino masses (in eV) used in this work for NH (left) and IH (right).

As will be seen, the mixing of the mass eigenstates with each flavor state is important to establish the optical depth, and therefore the horizon, for neutrino of different flavors.

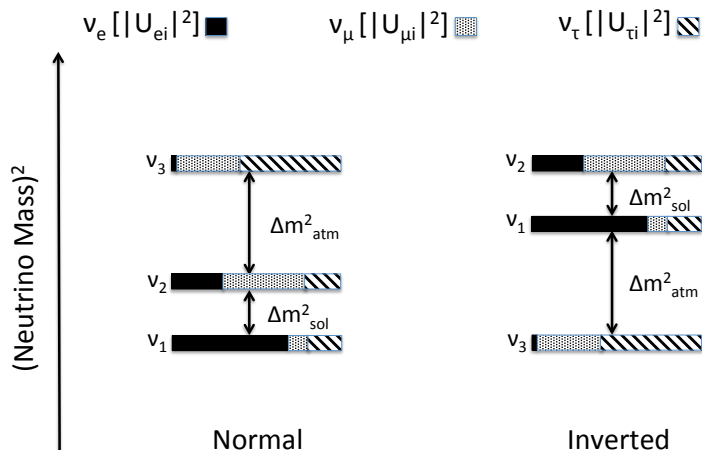


Figure 4. A graphical illustration of the mixing between mass and flavor eigenstates. The boxes represent the mass eigenstates, $i = 1, 2, 3$, the shaded regions represent their flavor admixtures $|U_{\alpha i}|^2$ for $\alpha = e, \mu, \tau$, $|\Delta m_{\text{atm}}^2| = |\Delta m_{31}^2| \approx |\Delta m_{32}^2| = 2.4 \times 10^{-3} \text{ eV}^2$ and $\Delta m_{\text{sol}}^2 = \Delta m_{21}^2 = 7.5 \times 10^{-5} \text{ eV}^2$.

The structure of the PMNS mixing matrix [47–49] $U_{\alpha i}$ depends on three angles, θ_{ij} , with $\sin^2 \theta_{12} \simeq 0.31$, $\sin^2 \theta_{23} \simeq 0.42$, and $\sin^2 \theta_{13} \simeq 0.025$ [46]. The fact that θ_{23} is very close to $\pi/4$, while θ_{13} is relatively small, makes it so that ν_3 is nearly a 50-50% mixture of ν_μ and ν_τ with a small ν_e component, while ν_1 and ν_2 have large admixtures of all the three flavors (Fig. 4).

2.3 Cosmic neutrino background

We assume a Friedmann Roberston Walker (FRW), Λ CDM universe, with the Hubble parameter

$$H(z) = \frac{\dot{a}}{a} = H_0 \sqrt{\Omega_m(1+z)^3 + \Omega_\Lambda}, \quad (2.1)$$

where $H_0 = 70.4 \text{ Mpc/km/s}$, $a = 1/(1+z)$ is the scale factor, z is the cosmological redshift, $\Omega_m = 0.272$ and $\Omega_\Lambda = 0.728$ are the fraction of the energy density of matter and dark energy respectively [50]. We also use natural units, $c = \hbar = 1$, and set Boltzmann's constant $k = 1$. The relationship between the proper time, t , and the redshift, z , is given by:

$$dt = \frac{dz}{(1+z)H(z)}, \quad (2.2)$$

and the comoving distance is

$$dr = \frac{dz}{H(z)}, \quad (2.3)$$

so that the comoving volume is given by

$$dV_c = r^2 dr d\Omega, \quad (2.4)$$

where $r = r(z)$ is the integral of Eq. (2.3) from present epoch to redshift z . Thus, the physical volume is simply $dV(z) = dV_c/(1+z)^3$.

Standard cosmology predicts the relic abundance of neutrinos with a thermal spectrum, similar to the cosmic microwave background (CMB) photons. Thermal equilibrium is provided by weak interactions, hence the relic neutrinos are produced in flavor eigenstates.

The number density of the CνB for a single neutrino species, is given by the Fermi-Dirac distribution (assuming zero chemical potentials) at temperature T as¹

$$dn(p, T) = \frac{d^3p}{(2\pi)^3} \frac{1}{e^{p/T} + 1} , \quad (2.5)$$

with p being the neutrino momentum. Because both p and T scale as $(1+z)$, dn simply scales as $d^3p \propto (1+z)^3$.

A neutrino is produced via the weak interaction as a flavor eigenstate, $|\nu_\alpha\rangle$. This state is a linear combination of mass (energy) eigenstates, $\{|\nu_j\rangle\}$, so that the time evolved freely streaming flavor ket has the form

$$|\nu_\alpha(t)\rangle = \sum_{j=1}^3 U_{\alpha j}^* e^{-i\Phi_j(t)} |\nu_j\rangle , \quad (2.6)$$

where $\Phi_j(t) = \int_{t_i}^t dt' \sqrt{[p(t')]^2 + m_j^2}$, and t_i is the neutrino production time. As the neutrino propagates onward, its three mass eigenstate components drift along with different velocities (due to their different masses). Therefore, given enough time, they would eventually become spatially separated, so that the coherence of the neutrino wavepacket is lost. When and how decoherence occurs for the CνB depends on the size of the neutrino wavepacket at decoupling, and on the neutrino mass spectrum; it has been studied only in part [51–53], with the general conclusion that, for a hierarchical mass spectrum, decoherence should have taken place between the neutrino horizon and today. Here we postpone a detailed description of neutrino decoherence, and consider the CνB to be in mass eigenstates, in accordance with previous literature [9]. We expect that a more accurate treatment of the quantum state of the CνB might perhaps change some quantitative details, but maintain the general features of the absorption pattern and the main conclusions of our work.

Let us now estimate when thermal effects are important. A given mass eigenstate (or, better, most of its population) is non-relativistic at $z \lesssim z_{\text{th},j}$:

$$1 + z_{\text{th},j} \sim \frac{m_j}{\bar{p}_0} \sim 16 \left(\frac{m_j}{10^{-2} \text{ eV}} \right) . \quad (2.7)$$

where $\bar{p}_0 = \sqrt{\langle p^2 \rangle} = 3.597 T_0 = 6.1044 \times 10^{-4} \text{ eV}$ and $T_0 = 1.697 \times 10^{-4} \text{ eV}$ is the CνB temperature at present epoch. Eq. (2.7) means that the heaviest mass eigenstate ($m \gtrsim 0.05 \text{ eV}$) is non-relativistic at $z \lesssim 83$. It is immediate to see that for $z \gtrsim z_{\text{th},j}$ thermal effects should be substantial for the ν_j component of the CνB in the scattering with UHE neutrinos. Therefore Eq. (2.7) offers a good guidance of the range of production redshifts where these effects should be included. The numerical results in the next section confirm this rough estimate.

3 Neutrino absorption effects

There are several propagation effects that leave imprints on the observed UHE neutrino fluxes. Since they are ultrarelativistic, their energy redshifts due to the expansion of the universe. Oscillations change the flavor composition of the neutrino flux, generally in the

¹After neutrino decoupling, T is actually *defined* by Eq. (2.5).

direction of flavor democracy, where all flavors are equally represented. Neutrinos are also absorbed due to resonant and non-resonant scatterings on the $C\nu B$. As a result of all these processes, the observed neutrino flux can differ significantly from the one at the production point. Here we focus on absorption, and incorporate the other effects as needed. The effect of cosmological redshift is included, and oscillations are modeled at the basic level by assuming flavor equipartition. As it will be shown, this is sufficient because the results are not very sensitive to the flavor composition of the UHE flux.

3.1 Cross sections

Several channels contribute to the process $\nu + \bar{\nu} \rightarrow \text{anything}$ [8, 11]. Their contributions to the total cross section, $\sigma_i(E, p, m_j, z)$ (with i indicating various channels), are summarized in Appendix A, and shown in Fig. 5.

These cross sections depend on the physics of the colliding neutrinos through the Mandelstam variable,

$$s = (q^\mu + p^\mu)^2 \approx 2E' \left(\sqrt{p^2 + m_j^2} - p \cos \theta \right), \quad (3.1)$$

$$q^\mu = [E', \mathbf{q}], \quad (3.2)$$

$$p^\mu = \left[\sqrt{p^2 + m_j^2}, \mathbf{p} \right], \quad (3.3)$$

where q^μ and p^μ are the four momenta of the UHE neutrino (“beam neutrino” from here on) and the background neutrino respectively, and $\mathbf{q} \cdot \mathbf{p} \equiv p q \cos \theta$. We use the approximation $E' = q$, since $q \gg m_j$ for the beam neutrino.

There are two qualitatively different channels that contribute to the scattering of UHE neutrinos on the $C\nu B$. The resonant channels correspond to annihilation of an UHE neutrino (antineutrino) with a background antineutrino (neutrino) via a Z^0 -resonance in the s-channel. The resonance occurs at $\sqrt{s} = M_Z$, where $M_Z = 91.1876$ GeV is the Z^0 boson mass, hence it is sensitive to the value of the neutrino mass, m_j , as well as the background neutrino momentum, p . Although the details can be complicated (see Appendix A), the main dependence of the total cross section on s , and therefore on q^μ and p^μ shows three regimes (see Fig. 5):

1. *Sub-resonance*: the cross section depends linearly on the energy of the beam neutrino, E' .
2. *At or near resonance*: the cross section is dominated by the resonant term, which has the characteristic Breit-Wigner enhancement.
3. *Above resonance*: the non-resonant cross sections approach an asymptotic value $\sigma_{\text{nr}} \sim 10^{33} \text{ cm}^2$.

In Fig. 5, these regimes are shown for the simplest and the most discussed case of the background neutrino at rest, i.e., $m_j \gg p$, which is realized for the $C\nu B$ at the present time and $m_j \gtrsim 10^{-3}$ eV. In this limit, $s \approx 2E'm_j$, therefore the resonance energy, $E'_{\text{res}} \approx M_Z^2/(2m_j)$ is a clear identifier of the neutrino mass.

The situation is less transparent in the most general case, where the momentum of the background neutrinos is not negligible, and thus the exact form of s given by Eq. (3.1) must be used. This is the central purpose of our study: to work out the phenomenology of neutrino absorption in its generality, and apply it to realistic examples. To do so, we have studied,

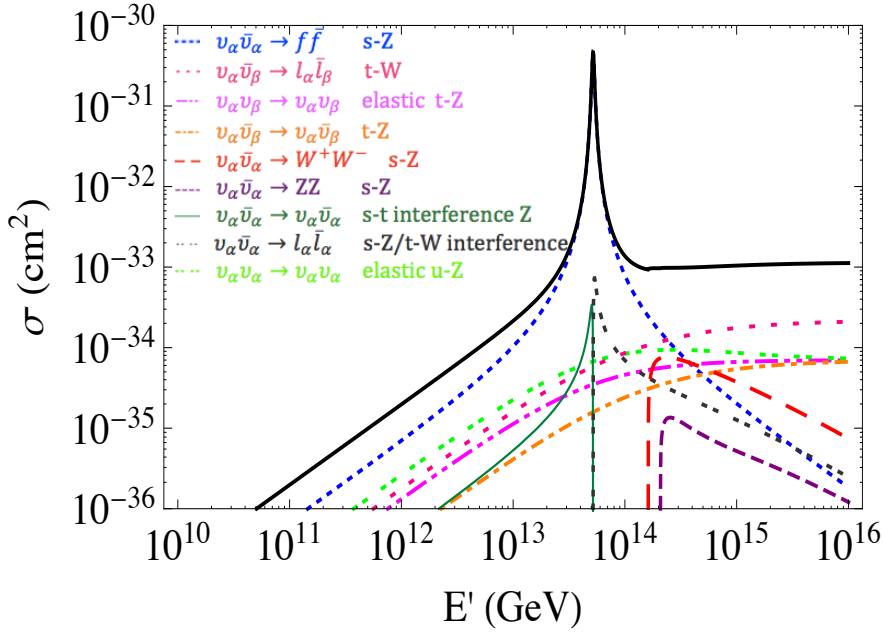


Figure 5. Contributions to the cross section for the processes $\nu + \bar{\nu} \rightarrow \text{anything}$. Various channels are shown with thin (colored) lines (see the legend in the figure), and the total cross section is shown with a thick (black) line for a representative neutrino mass of $m_\nu = 0.08$ eV. Thermal effects are not included.

for the resonant channels:

1. *The differential cross section $d\sigma_Z/d\Omega$.* This depends on θ through s , given by Eq. (3.1) (see also Appendix A). Since the C ν B is isotropic, we will only need the total cross section, σ_Z , obtained by integrating $d\sigma_Z/d\Omega$ over the angular variables. The result [10] is given in Appendix A. Although its explicit expression is complicated, its main features can be understood considering that now the resonance is realized for an interval of the beam neutrino energy, corresponding to θ varying between 0 and π [see Eq. (3.1)]. This results in a spread in the resonance peak compared to the background at rest (see Fig. 1). The cross section at resonance is larger for a head-on collision, $\theta = \pi$. This is because, there, the energy E' required to realize the resonance is minimum, and therefore the prefactor $1/E'$ in the cross section [Eq. (A.2)] is less suppressed.
2. *The momentum-averaged cross section.* The calculation of the neutrino optical depth (Sec. 3.2) requires the convolution of the total cross section σ_Z for a given momentum of the background neutrino with the momentum distribution of the C ν B [Eq. (2.5)]:

$$\bar{\sigma}_Z(E', T, m_j) = \frac{\int \sigma(E', p, m_j) dn(p, T)}{\int dn(p, T)}. \quad (3.4)$$

We have performed this calculation numerically for a wide range of beam energies and neutrino background temperatures. The results are illustrated in Fig. 6. We see that, as expected, the effect of including the momentum distribution of the background makes

the resonant peak smoother and broader: in addition to the broadening due to the angular integration, here the momentum distribution of the background further widens the range of beam energy where the resonance can be realized.

As the figure shows, the thermal effects on $\bar{\sigma}_Z(E', T, m_j)$ vary from negligible to substantial as the neutrino mass varies from much larger to comparable to the root mean square of the $C\nu B$ momentum, \bar{p} , or, for a fixed neutrino mass, as the temperature rises so that \bar{p} becomes comparable to the mass. Hence, the thermal effects become important at redshifts larger than $z_{\text{th},j}$ as in Eq. (2.7).

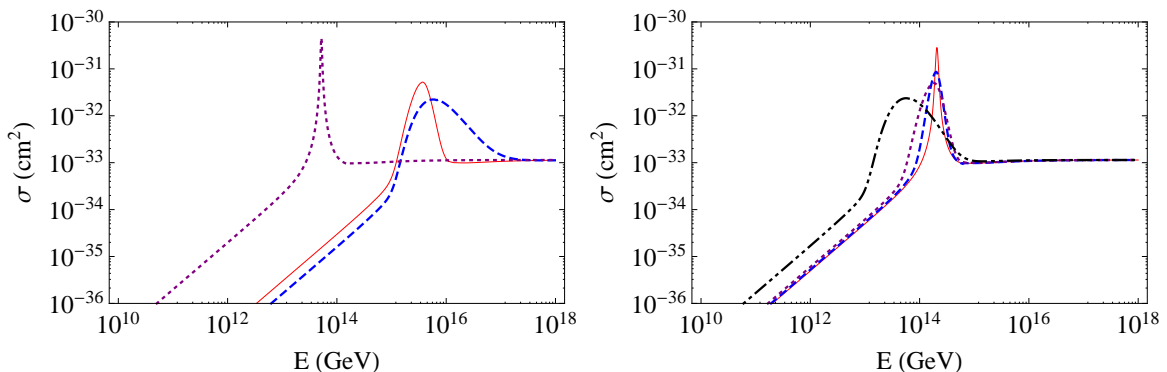


Figure 6. Left panel: the total ($\nu + \bar{\nu} \rightarrow \text{anything}$) cross section, inclusive of thermal effects, when averaged over a neutrino background with a momentum distribution as in Eq. (2.5), with temperature $T_0 = 1.697 \cdot 10^{-4}$ eV. Different lines correspond to neutrino masses: $m_\nu/\text{eV} = 8 \times 10^{-2}$ (purple – dotted), 10^{-3} (solid – red), 10^{-5} (dashed – blue). Right panel: the same cross section, for the neutrino mass of $m_\nu = 2 \times 10^{-2}$ eV and a neutrino background with temperatures $T/\text{eV} = 3.394 \times 10^{-4}, 1.867 \times 10^{-3}, 3.56 \times 10^{-3}, 1.713 \times 10^{-2}$ corresponding to $z = 1$ (red – solid), 10 (blue – dashed), 20 (purple – dotted), 100 (black – dash – dotted).

The momentum-averaged cross section gives a fully realistic description, that can be compared with some approximate treatments of the problem, shown in Fig. 1. In order of sophistication, they include: (i) neglecting the background neutrino momentum altogether, which overestimates the energy of the resonant enhancement (ii) including the background temperature in the form of an effective neutrino mass $m_{\text{eff},j} \simeq \sqrt{\bar{p}^2 + m_j^2}$, which reproduces the position of the resonance peak, and (iii) using the total cross section for the background neutrino momentum fixed at its root mean square value and averaged over the scattering angle. This captures in part the spread of the resonance peak over a range of energies. This range is further broadened for the full result, $\bar{\sigma}$.

In addition to the resonant channel, the non-resonant ones are considered as well, as summarized in Appendix A. Rigorously, one should repeat the considerations above to calculate the contributions of these channels. However, these non-resonant contributions are smooth functions of s , therefore we expect that the smearing effect due to the background temperature is well captured by using an averaged value of s instead of the exact expression in Eq. (3.3):

$$\bar{s}(E', m_j) \sim 2E' \sqrt{\bar{p}^2 + m_j^2}. \quad (3.5)$$

For simplicity, we use this prescription to calculate the contribution of the non-resonant channels to the total momentum-averaged cross section, $\bar{\sigma}_{\text{nr}}(E', m_j) = \sum_i \sigma_{\text{nr},i}(\bar{s})$, where $\sigma_{\text{nr},i}(s)$ is the non-resonant cross section for a given channel, i (Appendix A).

3.2 Optical depth and flux suppression

From the results of the previous section, it is immediate to find the scattering rate of a beam neutrino of energy E' and flavor α in a neutrino background of momentum p , whose distribution is given by Eq. (2.5) (see Appendix B for derivation):

$$\begin{aligned} \Gamma_\alpha(E', T) &= \sum_j |U_{\alpha j}|^2 \int \sigma(E', p, m_j) dn(p, T) \\ &\equiv \sum_j |U_{\alpha j}|^2 n(T) \bar{\sigma}(E', T, m_j), \end{aligned} \quad (3.6)$$

where the sum is over all mass eigenstates, j , and $n(T) = \int dn(p, T)$ is the number density of each neutrino species (assumed to be the same for all species).

The next step is to calculate the optical depth – i.e., the total number of collisions of an UHE neutrino of flavor α with the $C\nu B$ neutrinos throughout its path – considering that the energy of the beam and the momentum and temperature of the background undergo redshift. For convenience, in what follows T_0 is the temperature of the $C\nu B$ today, and E will represent the energy of the beam neutrino at Earth, i.e., $E = E'/(1+z)$. In these terms, the optical depth for a neutrino produced at redshift z can be written as:

$$\tau_\alpha(E, z) = \int_{t(z)}^{t_0} dt' \Gamma_\alpha[E(1+z'), T_0(1+z')] = \int_0^z \frac{dz'}{(1+z')H(z')} \Gamma_\alpha[E(1+z'), T_0(1+z')]. \quad (3.7)$$

Let us estimate for what values of z absorption is significant, i.e., $\tau_\alpha \gtrsim 1$. The total non-resonant cross section at $s \gtrsim m_W^2$ is approximately $\sigma_{\text{nr}} \approx \sigma_{tZ} + \sigma_{tW} \approx 7.8 G_F^2 m_W^2/\pi \sim 8.3 \times 10^{-34} \text{ cm}^2$ [see Eqs. (A.6) and (A.8)]. Using this value as a constant in Eq. (3.7), one gets

$$\tau_{\text{nr}} \approx 1.0 \left(\frac{1+z}{140} \right)^{3/2}. \quad (3.8)$$

Therefore, provided that $s \gtrsim m_W^2$, neutrinos are completely absorbed at all energies at $z \gtrsim z_\nu \approx 140$ due to non-resonant scatterings. Thus, we shall call z_ν as the neutrino horizon beyond which no neutrinos can propagate to us. Similarly, by using the maximum value of the resonant cross section, $\sigma_r \sim 5 \times 10^{-32} \text{ cm}^2$ [Eq. (A.4)], we get an estimate of the optical depth for the resonant channels:

$$\tau_r \approx 1.0 \left(\frac{1+z}{10} \right)^{3/2}. \quad (3.9)$$

Thus, resonant absorption occurs if the beam energy is around the resonant energy $E'_{\text{res}} \sim m_Z^2/\sqrt{\bar{p}_0^2(1+z)^2 + m_j^2}$ at $z \gtrsim z_{\text{dip}} \approx 10$.

From the optical depth, we obtain the suppression that applies to a flux of neutrinos ν_α , produced at redshift z and arriving at Earth with energy E :

$$P_\alpha(E, z) = e^{-\tau_\alpha(E, z)}. \quad (3.10)$$

Assuming that UHE neutrino detectors are flavor-blind, the relevant quantity is the suppression of the total flux, defined by the flux-averaged transmission probability:

$$P(E, z) \equiv \frac{\sum_{\alpha} \phi_{\alpha}(E) P_{\alpha}(E, z)}{\sum_{\alpha} \phi_{\alpha}(E)}, \quad (3.11)$$

with $\phi_{\alpha}(E)$ being the flux of neutrinos and antineutrinos of a given flavor α (under the assumption that neutrinos and antineutrinos have the same transmission and oscillation probabilities, which is justified for a CP-symmetric neutrino background)². For definiteness, we consider a flavor-democratic composition, with $\phi_e : \phi_{\mu} : \phi_{\tau} = 1 : 1 : 1$ at all energies, which is realized in many cases, at least approximately, due to flavor oscillations. This gives the simplest expression for P :

$$P(E, z) = \frac{1}{3} \sum_{\alpha} P_{\alpha}(E, z). \quad (3.12)$$

We note that $P_{\mu} \sim P_{\tau}$ are similar due to the structure of the neutrino mixing matrix, with maximal $\nu_{\mu} - \nu_{\tau}$ mixing. Therefore a result close to Eq. (3.12) is valid for different values of the ratio ϕ_{μ}/ϕ_{τ} , e.g., for $\phi_e : \phi_{\mu} : \phi_{\tau} = 1 : 2 : 0$, which is expected at production (i.e., before oscillations) for neutrino generation mechanisms via pion decays.

The main features of P_e, P_{μ}, P_{τ} and P are shown in Fig. 7. In principle, we expect each of these probabilities to exhibit three suppression dips, which we name D_1, D_2, D_3 , corresponding to the three values of the neutrino masses, m_1, m_2, m_3 . The order of the dips with increasing energy is the inverse of the order of masses, therefore the order is D_3, D_2, D_1 for NH and D_2, D_1, D_3 for IH. For z larger than a few, D_1 and D_2 appear fused into a single dip (D_{12}). This is due to the thermal effects, because the smaller mass gap is comparable with the neutrino average momentum, $m_2 - m_1 \lesssim 10^{-2}$ eV $\simeq \bar{p}$ at redshift $z = 10$. For P_e the dip D_3 is suppressed, as a result of U_{e3} being small (Sec. 2.2). This explains the dip structure of the flavor-averaged probability, P , and in particular the fact that the lowest energy dip is less deep for NH than for IH.

In Fig. 8, the dependence of P on the energy and on the production redshift is illustrated in more detail. The figure shows how resonant absorption becomes substantial ($P \lesssim 0.5$) for $z \gtrsim 10$, as expected from Eq. (2.7). For the same redshift, absorption above the resonance starts to have some effect, of about 10%. For $z \sim 50 - 100$, the three absorption dips merge into a single wide suppression well, that spans more than one order of magnitude in energy; suppression in the regime above resonance ($s \gtrsim m_W^2$) is of more than 50%. Finally, for $z \sim 200$, suppression is nearly complete at $E \gtrsim 10^{11}$ GeV, where the non-resonant contribution to the cross section alone is enough to have $\tau(E, z) > 1$.

4 Ultra high energy neutrino flux

Excluding the fortuitous case of a neutrino source near Earth, UHE neutrinos are expected to be detected in the form of a diffuse flux from all the sources in the universe. To calculate

²In fact, the beam neutrinos are in a mixed flavor state, since they oscillate, with oscillation length $L_{\text{beam}} = 4\pi E'/|\Delta m^2|$. These oscillations average out in cosmological distances since $L_{\text{beam}}/H^{-1} \sim 3.7 \times 10^{-7} (1+z)^{-5/2} [E/(10^{12}\text{GeV})] (|\Delta m_{21}^2|/|\Delta m^2|) \ll 1$ for all redshifts, where H is the Hubble parameter at epoch z . In Appendix B, it is demonstrated that, as long as the background neutrino is in a mass eigenstate, the resonant cross section does not depend on the oscillation phase of the beam neutrino.

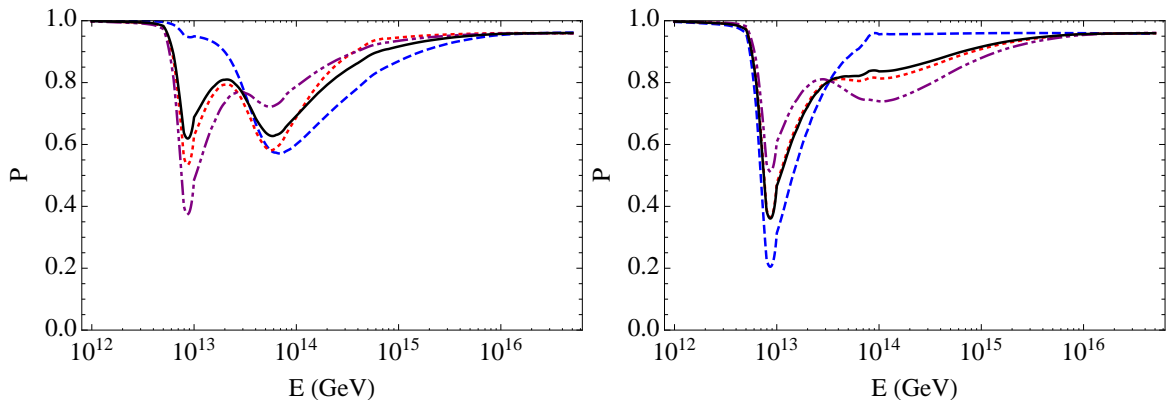


Figure 7. Transmission probabilities for UHE neutrinos with different flavors P_e, P_μ, P_τ [Eq. (3.11)] (dashed blue, dotted red, dash-dotted purple), and the average survival probability, P [Eq. (3.12)] (solid black), as a function of the energy, for a source at $z = 10$. Left (right) panel is for normal (inverted) hierarchy. The lightest neutrino has mass m_1 (m_3) = 10^{-5} eV.

this flux, it is necessary to model the number of sources per comoving volume, per unit of physical time, t :

$$\eta(z) \equiv \frac{1}{r^2} \frac{d^3 N_s}{d\Omega dr dt}, \quad (4.1)$$

and the neutrino flux from a single source:

$$\phi(E') \equiv \frac{dN_\nu}{dE'}. \quad (4.2)$$

The product of the two gives the emissivity of an ensemble of sources:

$$\mathcal{L}_\nu(E', z) = \eta(z)\phi(E'), \quad (4.3)$$

from which one gets the diffuse flux (i.e., the number of neutrinos per unit energy per unit area per unit time per solid angle), in terms of the energy of the neutrinos at Earth $E = E'/(1+z)$ [9]:

$$J_\nu(E) = \frac{1}{4\pi} \int_0^\infty \frac{dz}{H(z)} P(E, z) \mathcal{L}_\nu[E(1+z), z], \quad (4.4)$$

where Eq. (2.3) was used, and $P(E, z)$ is the average transmission probability given by Eq. (3.12).

Due to the integration over redshift, the suppression of the diffuse flux is less rich of structures compared to the case of a single source at fixed redshift. Therefore, we expect that only a single, wide suppression dip will appear in the neutrino spectrum. This suppression should be stronger for sources whose distribution extends to high redshifts, $z \gtrsim 10$, where $P \lesssim 0.5$ in the resonance region (see Fig. 8). In the next section, a number of specific examples are discussed.

4.1 Top down neutrino sources

Top down sources are objects predicted from physics beyond the standard model, that radiate light particles in a variety of mechanisms. The examples discussed here are topological defects, such as cosmic strings and cosmic necklaces, and unstable superheavy particles.

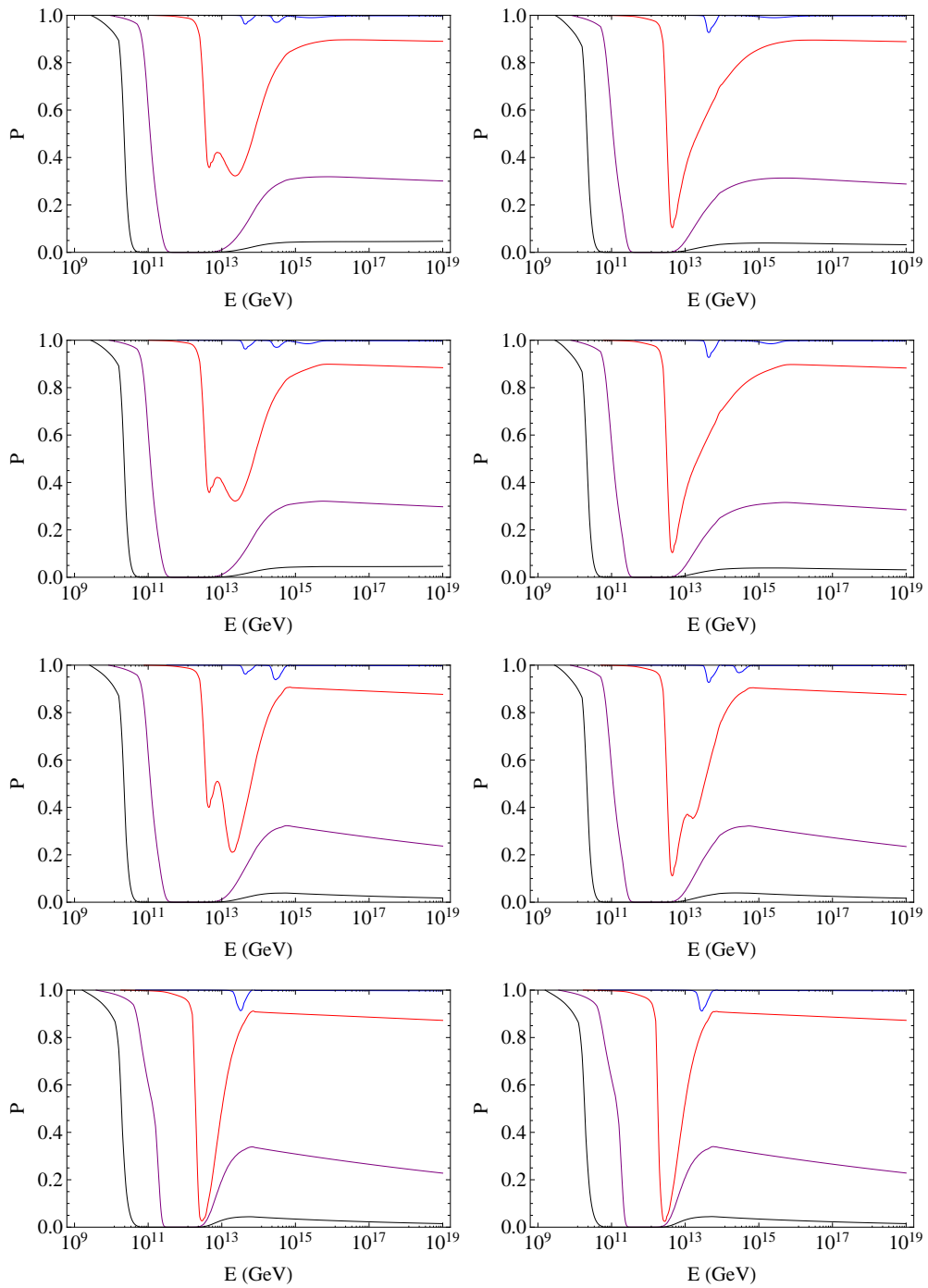


Figure 8. Flavor-averaged survival probability given by Eq. (3.12), as a function of the observed neutrino energy, for a source located at $z = 1$ (blue), 20 (red), 100 (purple), 200 (black) (curves from top to bottom in each figure). Left (right) column is for normal (inverted) hierarchy. Figures from top to bottom correspond to the lightest neutrino mass m_1 (m_3) in eV: 10^{-5} , 10^{-3} , 2×10^{-2} , 8×10^{-2} .

4.1.1 Cosmic strings

Cosmic strings are predicted in field theory models with spontaneous symmetry breaking whose vacuum manifold is not simply connected, e.g., Nielsen-Olesen topological strings in the Abelian Higgs model [54] (for reviews see, e.g., Refs.[55–58]). Cosmic F- and D-strings of superstrings theory may also be produced in the brane inflation models in string theory [59]. If they exist, cosmic strings are stable relics formed in the very early universe, thus, they have incredibly high energy densities in their core. They are characterized by their tension, μ (mass per unit length) denoted in Planck units as a dimensionless parameter $G\mu$, where G is Newton’s constant. The upper bound on cosmic string tension from CMB anisotropy measurements of WMAP and SPT is $G\mu \lesssim 1.7 \times 10^{-7}$ [60], and it has recently been updated by Planck to $G\mu \lesssim 1.5 \times 10^{-7}$ [61] which corresponds to a mass scale $m_s \lesssim \sqrt{\mu} \sim 5 \times 10^{15}$ GeV. This suggests that cosmic strings may be responsible for extremely high energy cosmic rays in the universe if they can emit particles efficiently.

Various mechanisms to produce particles from cosmic strings have been studied [62–69], but only a few of them yield observable fluxes. For instance, observable UHE neutrinos can be achieved at the cusps of superconducting cosmic strings [67], and at the cusps [68] and kinks [69] of cosmic strings and cosmic superstrings. Recently, Kaluza-Klein mode emission from cosmic superstring cusps has been shown to be an efficient radiation mechanism [70, 71], which can also lead to UHE neutrinos, and can be a potentially interesting signature of superstring theory.

In what follows, as an example, we discuss the case of neutrino emission from cosmic string cusps and kinks via heavy scalars (moduli) [67–69].

The neutrino emissivities from cusps [68] and kinks [69] (via modulus emission from cosmic strings) are respectively given by:

$$\mathcal{L}_\nu^{\text{cusp}} = 9.5 \times 10^{23} \frac{\alpha^2 (G\mu)^{1/2} \ln[(G\mu)^{1/2} m_p/m]}{p(1+z)^5} \frac{m_p}{E^2 t_p^{1/2} t(z)^{7/2}}, \quad (4.5)$$

$$\mathcal{L}_\nu^{\text{kink}} = 1 \times 10^{23} \frac{\alpha^2 (m_p/m)^{1/2}}{p(1+z)^5} \frac{m_p}{E^2 t(z)^4}, \quad (4.6)$$

where m_p is the Planck mass, t_p is the Planck time, $t(z)$ is the cosmic time given by the integral of Eq. (2.2) from epochs z to ∞ , $p \lesssim 1$ is the string reconnection probability, $G\mu$ is the string tension, m is the modulus mass and α is the modulus coupling constant. In both models, the neutrino production has a redshift cutoff,

$$z_{\text{min}}^{\text{str}} \sim 122 \left(\frac{G\mu}{10^{-17}} \right)^{2/7} \left(\frac{m}{10^4 \text{ GeV}} \right)^{2/7} \left(\frac{E}{10^{11} \text{ GeV}} \right)^{-4/7}, \quad (4.7)$$

that corresponds to the minimum energy at which the hadronic cascade produces pions ($\epsilon \sim 1$ GeV in the rest frame of the modulus), therefore the expressions above are valid for $z > z_{\text{min}}^{\text{str}}$. Eqs. (4.5) and (4.6) show that in both cases the emissivity is dominated by the emission at low redshifts, therefore the suppression of the diffuse flux due to absorption should be roughly determined by $P(E, z_{\text{min}}^{\text{str}})$. Here, we used the following parameter values: for kinks, $\alpha \sim 1$, $m \sim 10^4$ GeV, $G\mu \sim 10^{-17}$ and $p \sim 1$, corresponding to $z_{\text{min}}^{\text{str}} \simeq 2.3 - 122$ in the interval $E \simeq 10^{11} - 10^{14}$ GeV; for cusps, $\alpha \sim 2 \times 10^7$, $m \sim 10^4$ GeV, $G\mu \sim 6 \times 10^{-19}$ and $p \sim 1$, which give $z_{\text{min}}^{\text{str}} \simeq 1.0 - 54$ for $E \simeq 10^{11} - 10^{14}$ GeV.

Fig. 9 shows the diffuse flux from cosmic string kinks and cusps, with absorption effects, for the eight neutrino mass spectra (four for each hierarchy) listed in Table 1. The flux has

a sharp cutoff at about $E \sim 10^{10} - 10^{11}$ GeV. This is where the $z_{\min}^{\text{str}} \sim z_\nu \sim 140$, so that the entire flux is emitted beyond the neutrino horizon z_ν , and is completely absorbed before reaching Earth. In the spectrum, we observe the expected smearing of the dips into a single, broad suppression feature in the energy interval $E \sim 10^{11} - 10^{14}$ GeV. The suppression is overall stronger for kinks, due to the higher values of z_{\min}^{str} . The dependence of the suppression on the neutrino mass spectrum is fairly weak: the spectrum shape is nearly identical for the all cases except for the one with the largest mass. This is due to a combination of the two smearing effects discussed above, due to redshift integration and to the thermal effects. Considering large values of z_{\min}^{str} , thermal effects influence the position and depth of the dips more than the neutrino mass itself, at least for the strongly hierarchical neutrino spectra.

For superconducting string cusps, the neutrino emissivity is given by [67]

$$\mathcal{L}_\nu^{\text{sup}} = 1.4 \times 10^{22} \frac{i_c f_B}{(1+z)^{5/2}} \frac{B m_p t_p^{1/2}}{E^2 t(z)^{5/2}}, \quad (4.8)$$

where $i_c \lesssim 1$ is the dimensionless string parameter characterizing the maximum current on the string, $f_B \sim 10^{-3}$ is the magnetic field filling factor, $B \sim 10^{-6}$ G is the magnetic field strength. In Fig. 10, we take $i_c \sim 0.1$. Like in the previous case, the emissivity is dominated by low redshifts, and has a lower redshift cutoff,

$$z_{\min}^{\text{sup}} \sim 1.2 i_c^{3/2} \left(\frac{G\mu}{6.7 \times 10^{-19}} \right)^{-3/4} \left(\frac{B}{10^{-6} \text{ G}} \right)^2 \left(\frac{E}{10^{-12} \text{ GeV}} \right)^{-3/2}, \quad (4.9)$$

furthermore, $z < z_{\max} \sim 5$, because in Ref. [67], it was assumed that the magnetic fields trace galaxies and clusters, and thus strings have no current at times prior to structure formation.

In Fig. 10, we plot the neutrino flux from the superconducting cosmic string cusps. It can be clearly seen that the absorption dips are too tiny to be observable. Because the dominant redshift z_{\min}^{sup} is small, the optical depth is much less than unity, hence absorption is only at the level of 10% or less. Similarly to cosmic string cusp and kinks, the flux vanishes at about $E \sim 10^{11}$ GeV, when $z_{\min} \sim z_\nu$.

4.1.2 Cosmic necklaces

Cosmic necklaces are topological defects made up of strings and monopoles [72, 73]. They are predicted in field theory models, where the symmetry breaking sequence has the form $G \rightarrow H \times U(1) \rightarrow H \times Z_2$, where G is a semi-simple Lie group. As a result of the first symmetry breaking, monopoles form, and after the $U(1) \rightarrow Z_2$ breaking, each monopole is attached to two strings, each of which carries out half unit of flux as a result of the remaining Z_2 symmetry, hence the name cosmic necklace. As the monopoles and antimonopoles on loops of necklaces meet, they annihilate and produce heavy X -bosons related to the corresponding symmetry breaking scales of monopoles or strings. The bosons then decay via hadronic cascades into pions, that eventually decay producing numerous UHE neutrinos.

The neutrino emissivity from cosmic necklaces is given by [73] (see however Ref. [74])

$$\mathcal{L}_\nu^{\text{neck}} = \frac{\Theta[m_X - E(1+z)] e^{-E(1+z)/m_X}}{2 \ln[m_X/(1\text{GeV})] (1+z)^6} \frac{r}{E^2 m_p t_p t(z)^3}, \quad (4.10)$$

where m_X is the mass of the emitted heavy boson, and r is a parameter that depends on the monopole mass and the string tension. The model has a minimum redshift of neutrino

emission, z_{\min}^{neck} , which depends on the lifetime of the necklace. There is also a maximum energy cutoff, where $E' = E(1+z) \sim m_X$; the flux vanishes beyond this point. Here we take $m_X \sim 5 \times 10^{15}$ GeV, $r \sim 2 \times 10^{30}$ GeV² and $z_{\min}^{\text{neck}} = 10$.

Fig. 9 shows the diffuse flux expected in this model, with absorption included for the eight mass configurations of Table 1. The flux suppression effect is similar to the case of cosmic string cusps and kinks: all these models share the common feature of a large redshift cutoff, $z_{\min} \gtrsim 10$, which controls the degree of absorption. We note, however, that the cutoff is parameter-dependent: smaller values of z_{\min} (i.e., longer lifetime of the necklace) are allowed, and would result in weaker suppression. Even for large z_{\min}^{neck} , the flux from cosmic necklaces may show no absorption effects, if $m_X \lesssim 10^{12}$ GeV, which means that the maximum neutrino energy cutoff is below the range of energy where absorption is relevant.

4.1.3 Superheavy dark matter

The existence of dark matter is substantiated by various cosmological and astrophysical observations. Although we know the contribution of the dark matter particles to the cosmic energy density, $\Omega_{\text{CDM}} = 0.227$ [50] (expressed as a fraction of the critical density), their fundamental properties (mass, lifetime, spin, etc.) are still largely unknown, and are being tested via indirect and direct detection methods. Considering that the standard model has a zoo of particles of 3 families, it is natural to imagine that the dark matter sector may consist of multiple particle species. In this context, there could exist a long lived superheavy dark component – let’s call it X – with small abundance, i.e., $\Omega_{\text{SHDM}} \equiv \xi_X \Omega_{\text{CDM}}$ with $\xi_X \ll 1$ [3, 75–77]. The X particles may have masses up to of order GUT scale, $m_X \sim 10^{16}$ GeV. For them to be the thermal relics in the universe, m_X should be less than the reheating temperature, which can be constrained by the tensor to scalar ratio upper bounds to be around $T_{\text{rh}} \lesssim 5 \times 10^{15}$ GeV [78]. The life time τ_X of these objects can be as long as the age of the universe. However, if they decay via hadronic cascades somewhere between the neutrino horizon and today, a flux of UHE neutrinos should be generated.

The neutrino emissivity from decaying superheavy dark matter (SHDM) particles is given by [75]

$$\mathcal{L}_{\nu}^{\text{SHDM}} = \frac{3r_x \Omega_{\text{CDM}}}{16\pi} \frac{\Theta[m_X - E(1+z)] e^{-E(1+z)/m_X}}{\ln[m_X/(1\text{GeV})](1+z)^2} \frac{m_p H_0^2}{E^2 t_0 t_p}, \quad (4.11)$$

where $r_x \equiv \xi_X t_0 / \tau_X$. Here we use $m_X \sim 5 \times 10^{15}$ GeV, $r_x \sim 3 \times 10^{-7}$. The model has a minimum redshift, corresponding to the time where most of the X particles have decayed (assuming that their lifetime is shorter than the age of the universe). We use $z_{\min} = 10$.

Fig. 9 shows the resonant dips for different neutrino masses for SHDM whose emissivity is given by Eq. (4.11). Except for the different redshift dependence, this model is very similar to the cosmic necklace model since in both cases a heavy particle decays at rest, producing neutrinos via hadronic cascades. The same considerations done for cosmic necklaces apply here, and will not be repeated.

4.2 Astrophysical neutrino sources

4.2.1 Cosmogenic neutrinos

Cosmogenic neutrinos are a guaranteed result of UHE protons scattering off the background of (mostly CMB) photons [79]. This is the same phenomenon as the origin of the observed GZK cutoff of the cosmic ray proton spectrum [6, 7]. The neutrino production is dominated

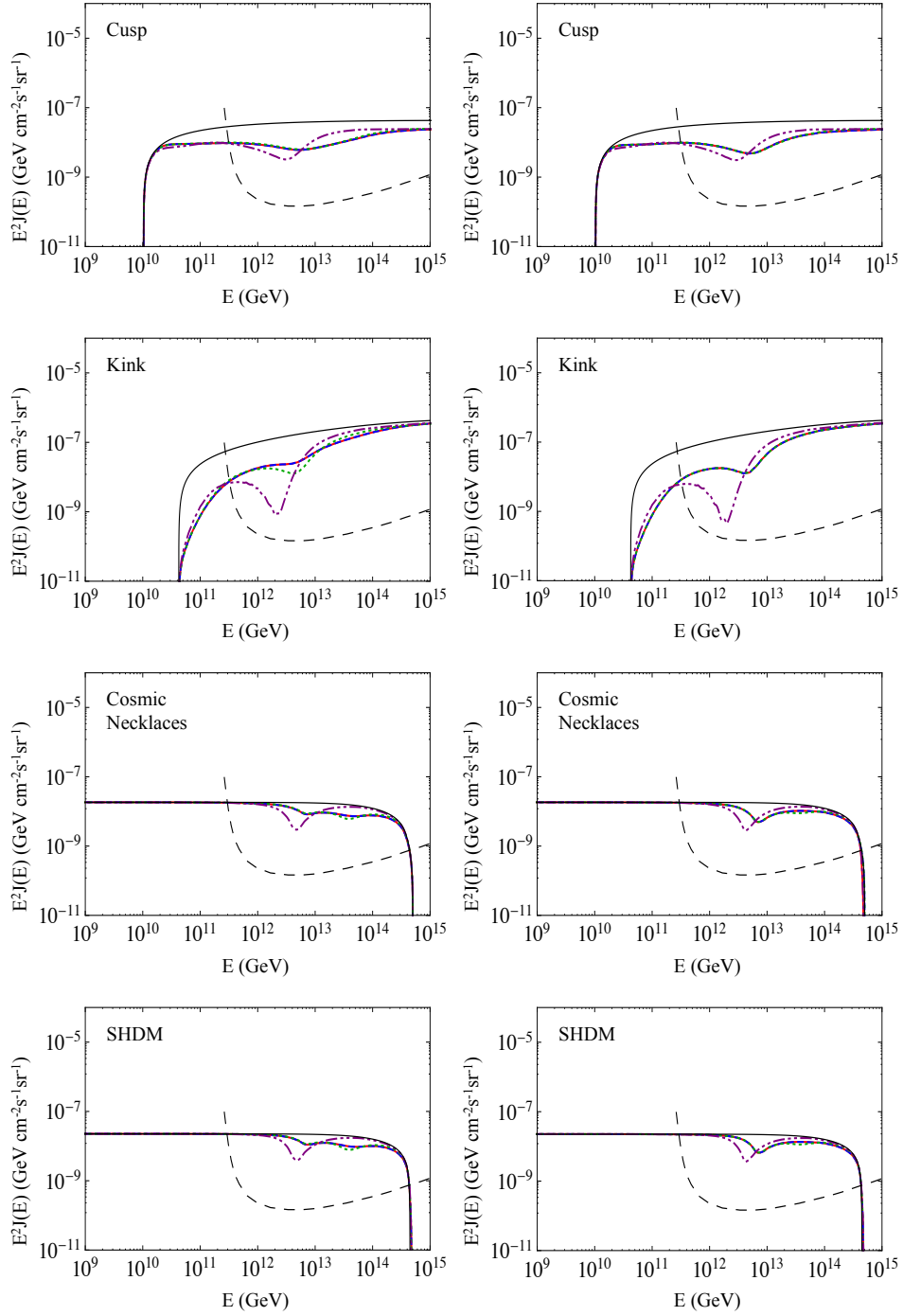


Figure 9. Expected neutrino fluxes from top down models: cosmic string cusps, kinks, cosmic necklaces and superheavy dark matter (SHDM) (labels in the figures), as a function of energy, for the neutrino masses given in Table 1. The curves correspond to different values of the minimum neutrino mass m_{\min} in eV: 10^{-5} (red, solid), 10^{-3} (blue, dashed), 2×10^{-2} (green, dotted), 8×10^{-2} (purple, dot-dashed). The left (right) column is for normal (inverted) hierarchy. Also shown are the fluxes with no absorption (thin, black solid) and the expected sensitivity of SKA (thin, black dashed).

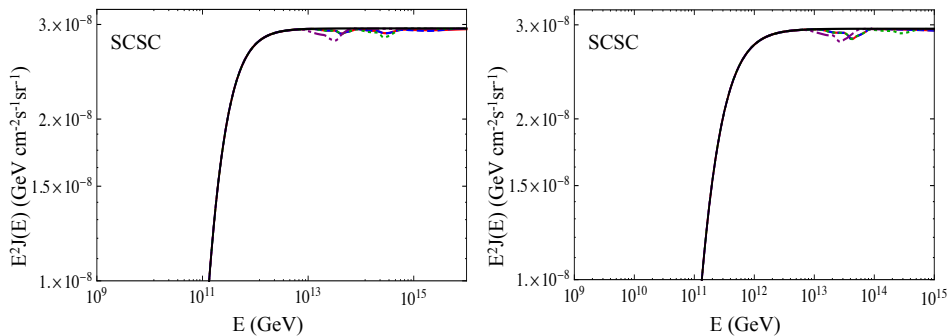


Figure 10. Expected neutrino flux from superconducting cosmic string cusps (SCSC) as a function of energy, for the same neutrino mass values (and color coding) as in Fig. 9. Left (right) column is for normal (inverted) hierarchy.

by the Δ^+ resonance, which for CMB photons is realized at $E_p \gtrsim 5 \times 10^{10}$ GeV of proton energy. Through the resonance, pions are produced, and their decay chain generates muon and electron neutrinos. Since the parent protons are absorbed efficiently, we expect that the neutrino flux can be higher than the observed proton one. The cosmogenic neutrino spectrum $\phi(E')$ has been calculated in Refs. [80, 81].

The neutrino emissivity for cosmogenic neutrinos is given by

$$\mathcal{L}_\nu^{\text{cosm}} = \mathcal{N}_0(1+z)^{n-1}\phi(E') \quad (4.12)$$

where \mathcal{N}_0 and n characterize the source population in normalization and redshift evolution. The neutrino spectrum $\phi(E')$ has an exponential cutoff at the maximum proton acceleration energy E_{max} .

Under the assumption that UHE protons are produced by stellar or galactic-size objects, the evolution of the source should have $n \simeq 3 - 4$, with a maximum redshift $z_{\text{max}} \simeq 7 - 10$. Here we take $n = 3$ and $z_{\text{max}} = 10$, and use the single source spectrum from Ref. [80], which has maximum acceleration energy $E_{\text{max}} \sim 10^{11}$ GeV. The resulting diffuse flux is shown in Fig. 2, and is practically the same with and without resonant absorption. Neutrino-neutrino scattering effects are completely negligible, since the sources are at low redshifts, $z_{\text{max}} \lesssim 10$, where the optical depth is very small, $\tau \ll 1$. Besides, even a modest absorption dip would probably be unobservable because the flux declines sharply with energy above E_{max} , and is greatly suppressed in the part of the spectrum relevant for absorption, $E \sim 10^{12} - 10^{13}$ GeV.

4.3 Gamma ray bursts and active galactic nuclei

Gamma ray bursts (GRB) and Active Galactic Nuclei (AGN) are sources of high energy gamma rays, and candidate sources of UHE neutrinos. The UHE neutrinos are produced via hadronic cascades in the interactions of high energy protons with the intense photon background in the source. The redshift evolution of these sources is believed to be stronger than the star formation rate history. Specifically, their comoving rate can be written as:

$$\frac{dN}{dz} = A \cdot \eta_{SFR}(z)(1+z)^\beta \frac{dV_c}{dz} \frac{1}{1+z}, \quad (4.13)$$

where V_c is the comoving volume, A is a normalization constant, and $\beta \simeq 1.5$ for GRB [82] and $\beta \simeq 2$ for AGN [83]. Here η_{SFR} is star formation rate density [84]:

$$\eta_{SFR}(z) = \eta_0 \left[(1+z)^a + \left(\frac{1+z}{B} \right)^b + \left(\frac{1+z}{C} \right)^c \right]^{-0.1}. \quad (4.14)$$

with $\eta_0 = 0.02 M_\odot \text{ yr}^{-1} \text{ Mpc}^{-3}$ (M_\odot is the mass of the Sun), $a = -34$, $b = 3$, $c = 3.5$, $B = 5000$, $C = 9$ [84].

The neutrino spectra follows a power law, $\phi(E') \propto E'^{-2}$, with a lower and upper energy cutoffs. Therefore the neutrino emissivity is given by,

$$\mathcal{L}_\nu^{\text{GRB}} = j_0 \frac{dN}{dz} \left(\frac{E(1+z)}{E_{\text{max}}} \right)^{-2} \Theta[E(1+z) - E_{\text{min}}] \Theta[E_{\text{max}} - E(1+z)]. \quad (4.15)$$

Here we use the normalization $j_0 \simeq 10^{-49} \text{ GeV cm/s}$, $E_{\text{min}} \simeq 10^9 \text{ GeV}$, and $E_{\text{max}} \simeq 10^{12} \text{ GeV}$ [9].

Similar to cosmogenic neutrinos, our results show that absorption is negligible for GRB and AGN neutrinos, since their flux is dominated by small redshifts of order a few, and is cut off below the energy range of interest for absorption.

5 Discussion

We have discussed the absorption of UHE neutrinos due to scattering on the $C\nu\text{B}$, with a focus on the effect of the thermal distribution of the background neutrinos. The thermal effects have been fully modeled, using realistic neutrino mass spectra and mixings. Neutrino absorption is dominated by the resonant Z^0 production. Thermal effects cause the resonance to be realized for an interval of the beam neutrino energy, depending on the scattering angle and the temperature of the background. As a consequence, the suppression of the UHE neutrino spectrum changes from sharp to wide as the thermal effects become important. This transition occurs when $\bar{p}(z) \sim m_{\text{min}}$, with m_{min} being the smallest of the three neutrino masses. In terms of cosmic time, this corresponds to redshift $1 + z_{\text{th}} \sim 16 m_{\text{min}} / (10^{-2} \text{ eV})$. For $m_{\text{min}} \lesssim 10^{-4} \text{ eV}$, thermal effects are already important, for the lightest neutrino species, at the present time. However, this does not translate in a flux suppression, due the insufficient optical depth. We find that the optical depth is substantial, $\tau \gtrsim 1$, for neutrino sources at $z \gtrsim 10$ [Eq. (3.9)].

The fact that $z \gtrsim 10$ is required to have significant suppression has two important consequences. First, neutrinos from stellar and galactic sources (e.g., cosmogenic neutrinos and neutrinos from AGN and GRBs), which extend up to $z \sim 5$ or so, have negligible absorption, and therefore their spectrum is a direct representation of the physics of the sources. Secondly, an observable spectrum distortion should have at most two dips, not three. This is because, at $z \gtrsim 10$, the mass difference between m_1 and m_2 is comparable with the average neutrino energy, i.e., $m_2 - m_1 \sim 10^{-2} \text{ eV} \simeq \bar{p}$, therefore the scattering off ν_1 and ν_2 causes a single dip instead of two separate ones.

A further smearing of the suppression dips is produced by integrating over the spatial distribution of the sources. We worked out specific examples of diffuse UHE neutrino fluxes, with a focus on neutrinos from top down mechanisms, for which the sources extend beyond $z \sim 10$, and therefore a strong absorption is expected. The cases considered were cosmic string kinks and cusps, super-heavy dark matter, cosmic necklaces and superconducting

strings. In all these models the flux is dominated by the contribution of sources closest to us, i.e., at the lowest redshift, z_{\min} , which, in general, depends on energy. Therefore, in first approximation the flux suppression is described by $P(E, z_{\min})$, with $P(E, z)$ being the probability of transmission for a neutrino of energy E (at Earth) and production epoch z [Eq. (3.12)]. We have found that, indeed, for sources with $z_{\min} \gtrsim 10$, the diffuse flux is suppressed strongly, up to an order of magnitude or even more, in some cases. A broad suppression valley is localized between 10^{12} and 10^{14} GeV; its shape and extent in energy depends on the details of the model and on the neutrino mass spectrum. However, the dependence on the neutrino mass spectrum, and especially on the mass hierarchy, is relatively weak. This generality is a result of the thermal effects, which, at least for the hierarchical mass spectra, dominate over the neutrino mass effect, and tend to make the suppression mass-independent. This has an immediate implication: the energy interval $10^{12} - 10^{13}$ GeV is potentially the worst place to look to discover UHE neutrinos! This might have to be taken into account in the design of UHE neutrino detectors. We note that SKA (which is not optimized for neutrino detection) has maximum sensitivity exactly in this range (see Fig. 2), therefore it might find itself in a position of disadvantage compared to other probes with different energy sensitivity.

Without being too specific, here we assume that UHE neutrino detectors can identify, at least roughly, a suppression in the neutrino spectrum. In the worst case of energy-blind detectors, some sensitivity can be gained by comparing the fluxes measurements or upper limits from different techniques probing different parts of the neutrino spectrum. For a single detector, a suppression may be defined only relative to a model of reference.

If UHE neutrinos are detected, and the data are compatible with a suppression due to neutrino absorption, what can be learned from them? Considering that the suppression bears only little dependence on the neutrino mass and mixing pattern, the main information will be on the physics of the sources. In particular, the observation of neutrino absorption will indicate, beyond doubt, a population of sources extending to $z \gtrsim 10$, earlier than the time of formation of stars and galaxies. Therefore, this might be a way to discover, or further substantiate, the existence of cosmological relics like superheavy dark matter, cosmic strings or necklaces. The detailed shape of the suppression dip (if available) would in principle allow to reconstruct z_{\min} as a function of energy since the distortion is roughly determined by $P(E, z_{\min})$. This can help to discriminate between different source models, if combined with other elements like the presence of a minimum energy cutoff (favoring cosmic string cusps and kinks) or a high energy flux termination (which would favor cosmic necklaces and superheavy dark matter).

Spectral distortions due to resonant absorption are, at least in principle, an interesting probe of the $C\nu B$ at relatively recent cosmological times, $z \sim 10 - 100$, that are out of the reach of both cosmological surveys [like those of Large Scale Structure ($z \lesssim 10$), and of the CMB ($z \sim 1100$), etc.] and direct detections of the $C\nu B$ (e.g., by zero-threshold nuclear decay [85], testing $z = 0$). In particular, an observed absorption pattern could help to constrain, or even reveal, several exotic effects:

(i) *Non standard neutrino number density.* An increased population of active neutrinos would result in stronger absorption dips. For example, we could consider an increase in number density by a factor $4/3$, corresponding to an effective number of cosmological relativistic degrees of freedom $N_{\text{eff}} = 4$, which has recently attracted some interest (see e.g., [44, 45]). This increase would change the optical depth by the same amount, and shorten the neutrino horizon down to $z \sim 120$. A depletion of the neutrino population at late times is also possible,

for example due to neutrino decay into a sterile neutrino or very weakly interacting species (e.g., [86]). This would suppress the absorption and extend the neutrino horizon.

(ii) *Non-standard neutrino spectrum.* Currently, there is no direct information on the $C\nu B$ spectrum, and indirect constraints are limited. Deviations from a thermal spectrum have been suggested, e.g., as a consequence of active-sterile neutrino conversion (e.g., [87]). They would influence the shape of the absorption dips, which could be narrower for a narrower neutrino spectrum or if the spectrum is much colder than expected, so to make most of the neutrinos non-relativistic at the epochs of interest.

(iii) *Neutrino asymmetry, anomalous flavor composition, non-standard neutrino interactions, and other exotica.* Our results could be generalized to consider a broader range of situations, including a neutrino population which is not flavor and CP-symmetric. Although these possibilities are interesting, to study them with UHE neutrino absorption may be complicated by degeneracies between the physics of the $C\nu B$ and the physics of the sources: for example, there is a degeneracy between the neutrino number density and the redshift distribution of the sources such that they both affect the depth of the spectral dips in a similar way.

If nothing else, it is important to accurately model the absorption dips to correctly interpret observations, and in particular to distinguish the effect of resonant $\nu-\bar{\nu}$ annihilation from spectral features of different nature, e.g., due to the overlap of two fluxes of different origin (bimodal spectrum), that could roughly mimic an absorption dip.

Although some of the effects described here require high precision and statistics, we can not underestimate the potential of this field to open a completely new way to explore the sky and learn about neutrinos.

A Cross sections

A.1 Resonant cross section

The resonant neutrino-antineutrino annihilation ($\nu\bar{\nu} \rightarrow Z^0 \rightarrow f\bar{f}$) occurs in the s-channel. The cross section is expressed as a function of the Mandelstam variable, $s = (q^\mu + p^\mu)^2$. Here $q^\mu = [E', \mathbf{q}]$ and $p^\mu = [\sqrt{\mathbf{p}^2 + m_j^2}, \mathbf{p}]$ are the four momenta of an UHE neutrino and background neutrinos, respectively. Since for UHE neutrinos $|\mathbf{q}| \gg m_{\nu_j}$, $E' \approx |\mathbf{q}| \equiv q$, then its four momentum is simply $q^\mu = E'[1, \hat{\mathbf{q}}]$. Note that in an expanding universe, we replace $E' = E(1+z)$ and $p = p_0(1+z)$, where E and p_0 are the values of the beam energy and background neutrino momentum at present epoch, respectively. Then, the Mandelstam variable, s , in the comoving frame is:

$$s(E', p, \theta) \approx 2E' \left[\sqrt{p^2 + m_j^2} - p \cos \theta \right], \quad (\text{A.1})$$

where $\hat{\mathbf{q}} \cdot \mathbf{p} \equiv p \cos \theta$. The differential cross section for the resonant s channel is [10]

$$d\sigma_{\text{r}}(E', p, s) = \frac{G_F \Gamma M_Z}{\sqrt{2} E' \sqrt{p^2 + m_{\nu_j}^2}} \frac{s(s - 2m_{\nu_j}^2)}{(s - M_Z^2)^2 + \xi s^2} ds, \quad (\text{A.2})$$

where $G_F = 1.16637 \times 10^{-5}$ GeV is the Fermi coupling constant, $M_Z = 91.1876$ GeV, $\Gamma = 2.495$ GeV is the width of the Z^0 resonance, $\xi = \Gamma^2/M_Z^2$. The total resonant cross section is obtained by integrating over s :

$$\sigma_{\text{r}}(E', p) = \int_{s_-}^{s_+} d\sigma_{\text{r}}(E', p, s), \quad (\text{A.3})$$

where $s_{\pm} \equiv 2E' \left[\sqrt{p^2 + m_j^2} \pm p \right]$ corresponding to head-on and parallel scattering, respectively. Eq. (A.3) can be expressed in an analytical form [10]

$$\begin{aligned} \sigma_r(E', p) &= \frac{G_F \Gamma M_Z}{\sqrt{2} E' \sqrt{p^2 + m_{\nu_j}^2}} \left[\frac{s}{1 + \xi} - \frac{M_Z^2 (\xi - 1)}{\sqrt{\xi} (1 + \xi)^2} \arctan \left(\frac{(1 + \xi) s - M_Z^2}{M_Z^2 \sqrt{\xi}} \right) \right. \\ &\quad \left. + \frac{M_Z^2}{(1 + \xi)^2} \ln \left[(1 + \xi) s^2 - 2M_Z^2 + M_Z^4 s \right] \right] \Big|_{s_-}^{s_+}, \end{aligned} \quad (\text{A.4})$$

where we take $s - 2m_{\nu_f}^2 \approx s$. The resonant cross section $\sigma_r(E', p)$ includes all kinematically allowed final states $(\bar{q}q, \bar{l}l)$, which is taken into account in the width Γ .

A.2 Non-resonant cross sections

Non-resonant cross sections are smooth functions of the beam energy E' , thus it is a very good approximation to use the value of s , averaged over scattering angle and momenta of the background neutrinos, instead of Eq. (A.1), to simplify the analysis:

$$\bar{s}(E', m_j) \equiv 2E' \sqrt{\bar{p}^2 + m_j^2}. \quad (\text{A.5})$$

All the relevant non-resonant processes are summarized as follows [8, 11]: The t-channel Z -exchange ($\nu_{\alpha} \bar{\nu}_{\beta} \rightarrow \nu_{\alpha} \bar{\nu}_{\beta}$) cross section with multiplicity 3 (including 3 different flavors for the target neutrino) is:

$$\sigma_{tZ} = 3 \frac{G_F^2 \bar{s}(E', m_j)}{2\pi} F_1(y_Z), \quad (\text{A.6})$$

where $F_1(y) = [y^2 + 2y - 2(1 + y) \ln(1 + y)]/y^3$ and $y_Z = \bar{s}(E', m_j)/M_Z^2$. For $\alpha = \beta$, there is an s-t interference term with multiplicity 1:

$$\sigma_{stZ} = \frac{G_F^2 \bar{s}(E', m_j)}{4\pi} F_2(y_Z) \frac{y_Z - 1}{(y_Z - 1)^2 + \Gamma^2/M_Z^2}, \quad (\text{A.7})$$

where $F_2(y) = [3y^2 + 2y - 2(1 + y)^2 \ln(1 + y)]/y^3$. The t-channel W -exchange ($\nu_{\alpha} \bar{\nu}_{\beta} \rightarrow l_{\alpha} \bar{l}_{\beta}$) cross section with multiplicity 3 is:

$$\sigma_{tW} = 3 \frac{2G_F^2 \bar{s}(E', m_j)}{\pi} F_1(y_W), \quad (\text{A.8})$$

where $y_W = \bar{s}(E', m_j)/M_W^2$ and $M_W = 80.385$ GeV. For $\alpha = \beta$, there is an interference between the s-channel Z -exchange and the t-channel W -exchange is with multiplicity 1:

$$\sigma_{stZW} = \frac{2G_F^2 (\sin^2 \theta_W - 1/2)}{\pi} y_W M_W^2 F_2(y_W) \frac{y_Z - 1}{(y_Z - 1)^2 + \Gamma^2/M_Z^2}, \quad (\text{A.9})$$

where $\sin^2 \theta_W = 0.23149$. The elastic t-channel Z -exchange ($\nu_{\alpha} \nu_{\beta} \rightarrow \nu_{\alpha} \nu_{\beta}$) cross section with multiplicity 3 is:

$$\sigma_{tZ}^{\text{el}} = 3 \frac{2G_F^2 M_Z^2}{2\pi} \frac{y_Z}{1 + y_Z}. \quad (\text{A.10})$$

There is also the u -channel Z -exchange that contributes to the same process ($\nu_{\alpha} \nu_{\beta} \rightarrow \nu_{\alpha} \nu_{\beta}$) with multiplicity 1:

$$\sigma_{uZ} = \frac{2G_F^2 \bar{s}(E', m_j)}{\pi} \left[\frac{1}{1 + y_Z} + \frac{\ln(1 + y_Z)}{y_Z(1 + y_Z/2)} \right]. \quad (\text{A.11})$$

The weak charged vector boson pair production cross section in the s -channel Z -exchange and the t -channel l -exchange ($\nu_\alpha \bar{\nu}_\alpha \rightarrow W^+ W^-$) with multiplicity 1 and threshold $s > 4M_W^2$ is:

$$\begin{aligned} \sigma_{WW} = & \frac{G_F^2 y_W M_W^2 \beta_W}{12\pi} \left[\frac{\beta_W^2 M_W^4}{M_Z^4 (y_Z - 1)^2} (12 + 20y_W + y_W^2) \right. \\ & + \frac{2M_W^2}{M_Z^2 (y_Z - 1) y_W^2} \left(24 + 28y_W - 18y_W^2 - y_W^3 + \frac{48(1 + 2y_W)L_W}{\beta_W y_W} \right) \\ & \left. + \frac{1}{y_W^2} \left(y_W^2 + 20y_W - 48 - \frac{48(2 - y_W)L_W}{\beta_W y_W} \right) \right], \end{aligned} \quad (\text{A.12})$$

where $\beta_W = \sqrt{1 - 4/y_W}$ and $L_W = \ln[(1 + \beta_W)(1 - \beta_W)]$. The weak neutral vector boson pair production cross section in the s -channel ($\nu_\alpha \bar{\nu}_\alpha \rightarrow ZZ$) with multiplicity 1 and threshold $s > 4M_Z^2$ is:

$$\sigma_{ZZ} = \frac{G_F^2 M_Z^2}{\pi} \frac{\beta_Z}{y_Z - 2} \left(\frac{2}{y_Z} - 1 + \frac{1 + y_Z^2}{2y_Z^2 \beta_Z} L_Z \right), \quad (\text{A.13})$$

where $\beta_Z = \sqrt{1 - 4/y_Z}$ and $L_Z = \ln[(1 + \beta_Z)(1 - \beta_Z)]$. Finally, ZH production cross section in the s -channel ($\nu_\alpha \bar{\nu}_\alpha \rightarrow Z^0 H$) with multiplicity 1 and threshold $s > (M_Z + M_H)^2$ is:

$$\sigma_{ZH} = \frac{G_F^2 M_Z^2}{96\pi} \frac{\sqrt{\lambda} \beta_Z}{y_Z} \frac{\lambda y_Z + 12}{(y_Z - 1)^2}, \quad (\text{A.14})$$

where $\lambda = [1 - (M_H + M_Z)^2/(y_Z M_Z^2)][1 - (M_H - M_Z)^2/(y_Z M_Z^2)]$ and $M_H = 125$ GeV. The total cross section is the sum of all the resonant and non-resonant channels, as shown in Fig. 5.

B Scattering amplitude and rate

In this appendix, we schematically show the dependence of the scattering rate on the neutrino mixing matrix for an UHE neutrino in a flavor eigenstate ν_α and a $C\nu B$ neutrino in a mass eigenstate ν_j , given by Eq. (3.6). For simplicity, consider the scattering amplitude for the s -channel process, $\nu_\alpha \bar{\nu}_j \rightarrow f \bar{f}$, where f is a final state fermion. The scattering amplitude $M_{\alpha j}$ is proportional to

$$M_{\alpha j} \propto \langle \bar{\nu}_j | O | \nu_\alpha \rangle = \sum_i U_{\alpha i}^* e^{-i\Phi_i(t)} \langle \bar{\nu}_j | O | \nu_i \rangle, \quad (\text{B.1})$$

where $U_{\alpha i}^*$ are the elements of the neutrino mixing matrix and $\Phi_i(t) = \int_{t_i}^t dt' \sqrt{[p(t')]^2 + m_i^2}$ is the quantum phase due to the neutrino propagation in vacuum between the time of production, t_i , and the time t when the collision occurs. This phase is responsible for neutrino flavor oscillations.

In eq. (B.1), the nonvanishing elements are the diagonal ones, i.e., $\langle \bar{\nu}_i | O | \nu_j \rangle \propto \delta_{ij} M_j$. Hence,

$$M_{\alpha j} \propto U_{\alpha j}^* e^{-i\Phi_j(t)} \langle \bar{\nu}_j | O | \nu_j \rangle \propto U_{\alpha j}^* e^{-i\Phi_j(t)} M_j. \quad (\text{B.2})$$

The corresponding cross section is then $\sigma(m_j) \propto |M_j|^2$. Note that the phase Φ_j cancels, hence neutrino oscillations do not affect the cross section provided that the background neutrino is

in mass eigenstate as we discussed in Sec. 2.3. Then, given dn as the number density of the $C\nu B$ neutrinos of each species, we have the scattering rate for an UHE neutrino of flavor α in the $C\nu B$ for a given process:

$$d\Gamma_\alpha = dn \sum_{j=1}^3 |U_{\alpha j}|^2 \sigma(m_j), \quad (\text{B.3})$$

which, after integration over the neutrino spectrum, recovers Eq. (3.6).

Acknowledgments

We would like to thank Ken Olum, Hiroyuki Tashiro and Tanmay Vachaspati for useful discussions. This work is supported in part by the National Science Foundation Grants No. PHY-0854827 and No. PHY-1205745 and Department of Energy at Arizona State University.

References

- [1] M. G. Aartsen *et al.* [IceCube Collaboration], *First observation of PeV-energy neutrinos with IceCube*, [[arXiv:1304.5356 \[astro-ph.HE\]](#)].
- [2] R. C. Gilmore, *Constraining the near-IR background light from Population-III stars using high redshift gamma-ray sources*, MNRAS, **420**, 1, (2012) 800-809 [[arXiv:1109.0592 \[astro-ph.CO\]](#)].
- [3] V. S. Berezinsky, *Neutrino astronomy and massive longlived particles from big bang*, Nucl. Phys. B **380** (1992) 478.
- [4] T. J. Weiler, *Resonant Absorption of Cosmic Ray Neutrinos by the Relic Neutrino Background*, Phys. Rev. Lett. **49** (1982) 234.
- [5] T. J. Weiler, *Big Bang Cosmology, Relic Neutrinos, And Absorption Of Neutrino Cosmic Rays*, Astrophys. J. **285** (1984) 495.
- [6] K. Greisen, *End to the cosmic ray spectrum?*, Phys. Rev. Lett. **16** (1966) 748.
- [7] G. T. Zatsepin and V. A. Kuzmin, *Upper limit of the spectrum of cosmic rays*, JETP Lett. **4** (1966) 78 [*Pisma Zh. Eksp. Teor. Fiz.* **4** (1966) 114].
- [8] E. Roulet, *Ultra-high-energy neutrino absorption by neutrino dark matter*, Phys. Rev. D **47** (1993) 5247.
- [9] B. Eberle, A. Ringwald, L. Song and T. J. Weiler, *Relic neutrino absorption spectroscopy*, Phys. Rev. D **70** (2004) 023007 [[hep-ph/0401203](#)].
- [10] J. C. D’Olivo, L. Nellen, S. Sahu and V. Van Elewyck, *UHE neutrino damping in a thermal gas of relic neutrinos*, Astropart. Phys. **25** (2006) 47 [[astro-ph/0507333](#)].
- [11] G. Barenboim, O. Mena Requejo and C. Quigg, *Diagnostic potential of cosmic-neutrino absorption spectroscopy*, Phys. Rev. D **71** (2005) 083002 [[hep-ph/0412122](#)].
- [12] G. A. Askaryan, Zh. Eksp. Teor. Fiz. **41**, (1961) 616 [*Soviet Physics JETP* **14**, (1962) 441]; G. A. Askaryan, Zh. Eksp. Teor. Fiz. **48**, (1965) 988 [*Soviet Physics JETP* **21**, (1965) 658].
- [13] D. Saltzberg, P. Gorham, D. Walz, C. Field, R. Iverson, A. O’Dian, G. Resch and P. Schoessow *et al.*, *Observation of the Askaryan effect: Coherent microwave Cherenkov emission from charge asymmetry in high-energy particle cascades*, Phys. Rev. Lett. **86** (2001) 2802 [[hep-ex/0011001](#)].

- [14] P. W. Gorham *et al.* [ANITA Collaboration], *Observations of the Askaryan effect in ice*, Phys. Rev. Lett. **99** (2007) 171101 [[hep-ex/0611008](#)].
- [15] P. W. Gorham, C. L. Hebert, K. M. Liewer, C. J. Naudet, D. Saltzberg and D. Williams, *Experimental limit on the cosmic diffuse ultrahigh-energy neutrino flux*, Phys. Rev. Lett. **93** (2004) 041101 [[astro-ph/0310232](#)].
- [16] S. Buitink, J. Bacelar, R. Braun, G. de Bruyn, H. Falcke, O. Scholten, K. Singh and B. Stappers *et al.*, *The NuMoon experiment: first results*, [[arXiv:0808.1878](#) [[astro-ph](#)]].
- [17] O. Scholten, S. Buitink, J. Bacelar, R. Braun, A. G. de Bruyn, H. Falcke, K. Singh and B. Stappers *et al.*, *First results of the NuMoon experiment*, Nucl. Instrum. Meth. A **604** (2009) S102.
- [18] S. Buitink, O. Scholten, J. Bacelar, R. Braun, A. G. de Bruyn, H. Falcke, K. Singh and B. Stappers *et al.*, *Constraints on the flux of Ultra-High Energy neutrinos from WSRT observations*, [[arXiv:1004.0274](#) [[astro-ph.HE](#)]].
- [19] T. R. Jaeger, R. L. Mutel and K. G. Gayley, *Project RESUN, a radio EVLA search for UHE neutrinos*, Astropart. Phys. **34** (2010) 293.
- [20] N. G. Lehtinen, P. W. Gorham, A. R. Jacobson and R. A. Roussel-Dupre, *FORTE satellite constraints on ultra-high energy cosmic particle fluxes*, Phys. Rev. D **69** (2004) 013008 [[astro-ph/0309656](#)].
- [21] S. W. Barwick *et al.* [ANITA Collaboration], *Constraints on cosmic neutrino fluxes from the anita experiment*, Phys. Rev. Lett. **96** (2006) 171101 [[astro-ph/0512265](#)].
- [22] P. W. Gorham *et al.* [ANITA Collaboration], *New Limits on the Ultra-high Energy Cosmic Neutrino Flux from the ANITA Experiment*, Phys. Rev. Lett. **103** (2009) 051103 [[arXiv:0812.2715](#) [[astro-ph](#)]].
- [23] M. Mottram [ANITA Collaboration], *An observational limit on the UHE cosmic neutrino flux from the second flight of the ANITA experiment*, Nucl. Instrum. Meth. A **662** (2012) S59.
- [24] I. Kravchenko, C. Cooley, S. Hussain, D. Seckel, P. Wahrlich, J. A. Adams, S. Churchwell and P. Harris *et al.*, *Rice limits on the diffuse ultrahigh energy neutrino flux*, Phys. Rev. D **73** (2006) 082002 [[astro-ph/0601148](#)].
- [25] O. Scholten, J. Bacelar, R. Braun, A. G. de Bruyn, H. Falcke, B. Stappers and R. G. Strom, *Optimal radio window for the detection of ultra-high-energy cosmic rays and neutrinos off the moon*, Astropart. Phys. **26** (2006) 219 [[astro-ph/0508580](#)].
- [26] O. Scholten, S. Buitink, H. Falcke, C. W. James, M. Mevius, K. Singh, B. Stappers and S. ter Veen, *Ultra-high-energy cosmic ray and neutrino detection using the Moon*, Nucl. Phys. Proc. Suppl. **212-213** (2011) 128.
- [27] S. Buitink *et al.* [LOFAR Collaboration], *Searching for Neutrino Radio Flashes from the Moon with LOFAR*, [[arXiv:1301.5185](#) [[astro-ph.IM](#)]].
- [28] C. W. James and R. J. Protheroe, *The sensitivity of the next generation of lunar Cherenkov observations to UHE neutrinos and cosmic rays*, Astropart. Phys. **30** (2009) 318 [[arXiv:0802.3562](#) [[astro-ph](#)]].
- [29] R. D. Ekers, C. W. James, R. J. Protheroe and R. A. McFadden, *Lunar radio Cherenkov observations of UHE neutrinos*, Nucl. Instrum. Meth. A **604** (2009) S106.
- [30] T. Ebisuzaki, Y. Uehara, H. Ohmori, K. Kawai, Y. Kawasaki, M. Sato, Y. Takizawa and M. E. Bertaina *et al.*, *The JEM-EUSO project: Observing extremely high energy cosmic rays and neutrinos from the International Space Station*, Nucl. Phys. Proc. Suppl. **175-176** (2008) 237.

- [31] Y. Takahashi [JEM-EUSO Collaboration], *The JEM-EUSO mission*, New J. Phys. **11** (2009) 065009.
- [32] G. Medina-Tanco *et al.* [JEM-EUSO Collaboration], *JEM-EUSO Science Objectives*, [[arXiv:0909.3766 \[astro-ph.HE\]](#)].
- [33] C. W. James, R. D. Ekers, J. Alvarez-Muniz, J. D. Bray, R. A. McFadden, C. J. Phillips, R. J. Protheroe and P. Roberts, *LUNASKA experiments using the Australia Telescope Compact Array to search for ultra-high energy neutrinos and develop technology for the lunar Cherenkov technique*, Phys. Rev. D **81** (2010) 042003 [[arXiv:0911.3009 \[astro-ph.HE\]](#)].
- [34] J. D. Bray, R. D. Ekers, R. J. Protheroe, C. W. James, C. J. Phillips, P. Roberts, A. Brown and J. E. Reynolds *et al.*, *LUNASKA neutrino search with the Parkes and ATCA telescopes*, [[arXiv:1301.6490 \[astro-ph.IM\]](#)].
- [35] L. Gerhardt, S. Klein, T. Stezelberger, S. Barwick, K. Dookayka, J. Hanson and R. Nichol, *A prototype station for ARIANNA: a detector for cosmic neutrinos*, Nucl. Instrum. Meth. A **624** (2010) 85 [[arXiv:1005.5193 \[astro-ph.IM\]](#)].
- [36] H. Landsman [AURA Collaboration], *AURA: Next generation neutrino detector in the South Pole*, Nucl. Phys. Proc. Suppl. **168** (2007) 268.
- [37] H. Landsman *et al.* [IceCube Collaboration], *AURA - A radio frequency extension to IceCube*, Nucl. Instrum. Meth. A **604** (2009) S70 [[arXiv:0811.2520 \[astro-ph\]](#)].
- [38] P. W. Gorham, F. E. Baginski, P. Allison, K. M. Liewer, C. Miki, B. Hill and G. S. Varner, *The ExaVolt Antenna: A Large-Aperture, Balloon-embedded Antenna for Ultra-high Energy Particle Detection*, Astropart. Phys. **35** (2011) 242 [[arXiv:1102.3883 \[astro-ph.IM\]](#)].
- [39] V. S. Berezinsky and A. Y. Smirnov, *Cosmic neutrinos of ultra-high energies and detection possibility*, Astrophys. Space Sci. **32** (1975) 461.
- [40] A. A. Abdo *et al.* [Fermi-LAT Collaboration], *The Spectrum of the Isotropic Diffuse Gamma-Ray Emission Derived From First-Year Fermi Large Area Telescope Data*, Phys. Rev. Lett. **104** (2010) 101101 [[arXiv:1002.3603 \[astro-ph.HE\]](#)].
- [41] V. Berezinsky, A. Gazizov, M. Kachelriess and S. Ostapchenko, *Restricting UHECRs and cosmogenic neutrinos with Fermi-LAT*, Phys. Lett. B **695** (2011) 13 [[arXiv:1003.1496 \[astro-ph.HE\]](#)].
- [42] C. Kraus, B. Bornschein, L. Bornschein, J. Bonn, B. Flatt, A. Kovalik, B. Ostrick and E. W. Otten *et al.*, *Final results from phase II of the Mainz neutrino mass search in tritium beta decay*, Eur. Phys. J. C **40**, 447 (2005) [[hep-ex/0412056](#)].
- [43] V. N. Aseev *et al.* [Troitsk Collaboration], *An upper limit on electron antineutrino mass from Troitsk experiment*, Phys. Rev. D **84**, 112003 (2011) [[arXiv:1108.5034 \[hep-ex\]](#)].
- [44] G. Hinshaw *et al.* [WMAP Collaboration], *Nine-Year Wilkinson Microwave Anisotropy Probe (WMAP) Observations: Cosmological Parameter Results*, [[arXiv:1212.5226 \[astro-ph.CO\]](#)].
- [45] P. A. R. Ade *et al.* [Planck Collaboration], *Planck 2013 results. XVI. Cosmological parameters*, [[arXiv:1303.5076 \[astro-ph.CO\]](#)].
- [46] G. L. Fogli, E. Lisi, A. Marrone, D. Montanino, A. Palazzo and A. M. Rotunno, *Global analysis of neutrino masses, mixings and phases: entering the era of leptonic CP violation searches*, Phys. Rev. D **86**, 013012 (2012) [[arXiv:1205.5254 \[hep-ph\]](#)].
- [47] B. Pontecorvo, *Mesonium and anti-mesonium*, Sov. Phys. JETP **6** (1957) 429 [Zh. Eksp. Teor. Fiz. **33** (1957) 549].
- [48] B. Pontecorvo, *Neutrino Experiments and the Problem of Conservation of Leptonic Charge*, Sov. Phys. JETP **26** (1968) 984 [Zh. Eksp. Teor. Fiz. **53** (1967) 1717].

- [49] Z. Maki, M. Nakagawa and S. Sakata, *Remarks on the unified model of elementary particles*, Prog. Theor. Phys. **28** (1962) 870.
- [50] E. Komatsu *et al.* [WMAP Collaboration], *Seven-Year Wilkinson Microwave Anisotropy Probe (WMAP) Observations: Cosmological Interpretation*, Astrophys. J. Suppl. **192** (2011) 18 [[arXiv:1001.4538](#) [[astro-ph.CO](#)]].
- [51] G. M. Fuller and C. T. Kishimoto, *Quantum Coherence of Relic Neutrinos*, Phys. Rev. Lett. **102** (2009) 201303 [[arXiv:0811.4370](#) [[astro-ph](#)]].
- [52] A. E. Bernardini and V. A. S. V. Bittencourt, *The $C\nu B$ energy density through the quantum measurement theory*, Astropart. Phys. **41** (2013) 31 [[arXiv:1210.7987](#) [[hep-ph](#)]].
- [53] S. Dodelson and M. Vesterinen, *Cosmic Neutrino Last Scattering Surface*, Phys. Rev. Lett. **103** (2009) 171301 [Erratum-ibid. **103** (2009) 249901] [[arXiv:0907.2887](#) [[astro-ph.CO](#)]].
- [54] H. B. Nielsen and P. Olesen, *Vortex Line Models for Dual Strings*, Nucl. Phys. B **61** (1973) 45.
- [55] A. Vilenkin and E.P.S. Shellard, *Cosmic Strings and Other Topological Defects*, Cambridge University Press, Cambridge (1994).
- [56] E. J. Copeland and T. W. B. Kibble, *Cosmic Strings and Superstrings*, Proc. Roy. Soc. Lond. A **466** (2010) 623 [[arXiv:0911.1345](#) [[hep-th](#)]].
- [57] J. Polchinski, *Introduction to cosmic F- and D-strings* [[hep-th/0412244](#)].
- [58] E. J. Copeland, L. Pogosian and T. Vachaspati, *Seeking String Theory in the Cosmos*, Class. Quant. Grav. **28** (2011) 204009 [[arXiv:1105.0207](#) [[hep-th](#)]].
- [59] S. Sarangi and S. H. H. Tye, *Cosmic string production towards the end of brane inflation*, Phys. Lett. B **536** (2002) 185 [[hep-th/0204074](#)].
- [60] C. Dvorkin, M. Wyman and W. Hu, *Cosmic String constraints from WMAP and the South Pole Telescope*, Phys. Rev. D **84** (2011) 123519 [[arXiv:1109.4947](#) [[astro-ph.CO](#)]].
- [61] P. A. R. Ade *et al.* [Planck Collaboration], *Planck 2013 results. XXV. Searches for cosmic strings and other topological defects*, [[arXiv:1303.5085](#) [[astro-ph.CO](#)]].
- [62] C. T. Hill, D. N. Schramm and T. P. Walker, *Ultra-high-Energy Cosmic Rays from Superconducting Cosmic Strings*, Phys. Rev. D **36** (1987) 1007.
- [63] P. Bhattacharjee, *Cosmic Strings and Ultra-high-Energy Cosmic Rays*, Phys. Rev. D **40** (1989) 3968.
- [64] J. H. MacGibbon and R. H. Brandenberger, *High-energy Neutrino Flux From Ordinary Cosmic Strings*, Nucl. Phys. B **331** (1990) 153.
- [65] R. Brandenberger, Y. -F. Cai, W. Xue and X. M. Zhang, *Cosmic Ray Positrons from Cosmic Strings*, [[arXiv:0901.3474](#) [[hep-ph](#)]].
- [66] T. Vachaspati, *Cosmic Rays from Cosmic Strings with Condensates*, Phys. Rev. D **81** (2010) 043531 [[arXiv:0911.2655](#) [[astro-ph.CO](#)]].
- [67] V. Berezhinsky, K. D. Olum, E. Sabancilar and A. Vilenkin, *UHE neutrinos from superconducting cosmic strings*, Phys. Rev. D **80** (2009) 023014 [[arXiv:0901.0527](#) [[astro-ph.HE](#)]].
- [68] V. Berezhinsky, E. Sabancilar and A. Vilenkin, *Extremely High Energy Neutrinos from Cosmic Strings*, Phys. Rev. D **84** (2011) 085006 [[arXiv:1108.2509](#) [[astro-ph.CO](#)]].
- [69] C. Lunardini and E. Sabancilar, *Cosmic Strings as Emitters of Extremely High Energy Neutrinos*, Phys. Rev. D **86** (2012) 085008 [[arXiv:1206.2924](#) [[astro-ph.CO](#)]].
- [70] J. -F. Dufaux, *Constraints on Cosmic Super-Strings from Kaluza-Klein Emission*, Phys. Rev. Lett. **109** (2012) 011601 [[arXiv:1109.5121](#) [[hep-th](#)]].

- [71] J. -F. Dufaux, *Cosmic Super-Strings and Kaluza-Klein Modes*, JCAP **1209** (2012) 022 [[arXiv:1201.4850](#) [hep-th]].
- [72] V. Berezhinsky, X. Martin and A. Vilenkin, *High-energy particles from monopoles connected by strings*, Phys. Rev. D **56** (1997) 2024 [[astro-ph/9703077](#)].
- [73] V. Berezhinsky and A. Vilenkin, *Cosmic necklaces and ultrahigh-energy cosmic rays*, Phys. Rev. Lett. **79** (1997) 5202 [[astro-ph/9704257](#)].
- [74] J. J. Blanco-Pillado and K. D. Olum, JCAP **1005** (2010) 014 [[arXiv:0707.3460](#) [astro-ph]].
- [75] V. Berezhinsky, M. Kachelriess and A. Vilenkin, *Ultrahigh-energy cosmic rays without GZK cutoff*, Phys. Rev. Lett. **79** (1997) 4302 [[astro-ph/9708217](#)].
- [76] V. A. Kuzmin and V. A. Rubakov, *Ultrahigh-energy cosmic rays: A Window to postinflationary reheating epoch of the universe?*, Phys. Atom. Nucl. **61** (1998) 1028 [Yad. Fiz. **61** (1998) 1122] [[astro-ph/9709187](#)].
- [77] D. J. H. Chung, E. W. Kolb and A. Riotto, *Production of massive particles during reheating*, Phys. Rev. D **60** (1999) 063504 [[hep-ph/9809453](#)].
- [78] P.A.R. Ade *et al.* [Planck Collaboration], *Planck 2013 results. XVI. Cosmological parameters*, [[arXiv:1303.5076](#) [astro-ph.CO]].
- [79] V. S. Berezhinsky and G. T. Zatsepin, *Cosmic rays at ultrahigh-energies (neutrino?)*, Phys. Lett. B **28** (1969) 423.
- [80] R. Engel, D. Seckel and T. Stanev, *Neutrinos from propagation of ultrahigh-energy protons*, Phys. Rev. D **64** (2001) 093010 [[astro-ph/0101216](#)].
- [81] O. E. Kalashev, V. A. Kuzmin, D. V. Semikoz and G. Sigl, *Ultrahigh-energy neutrino fluxes and their constraints*, Phys. Rev. D **66** (2002) 063004 [[hep-ph/0205050](#)].
- [82] B. E. Robertson and R. S. Ellis, *Connecting the Gamma Ray Burst Rate and the Cosmic Star Formation History: Implications for Reionization and Galaxy Evolution*, Astrophys. J. **744** (2012) 95 [[arXiv:1109.0990](#) [astro-ph.CO]].
- [83] G. Hasinger, T. Miyaji and M. Schmidt, *Luminosity-dependent evolution of soft x-ray selected AGN: New Chandra and XMM-Newton surveys*, Astron. Astrophys. **441** (2005) 417 [[astro-ph/0506118](#)].
- [84] H. Yuksel, M. D. Kistler, J. F. Beacom and A. M. Hopkins, *Revealing the High-Redshift Star Formation Rate with Gamma-Ray Bursts*, Astrophys. J. **683** (2008) L5 [[arXiv:0804.4008](#) [astro-ph]].
- [85] S. Weinberg, *Universal Neutrino Degeneracy*, Phys. Rev. **128** (1962) 1457.
- [86] J. F. Beacom, N. F. Bell and S. Dodelson, *Neutrinoless universe*, Phys. Rev. Lett. **93**, 121302 (2004) [[astro-ph/0404585](#)].
- [87] C. T. Kishimoto, G. M. Fuller and C. J. Smith, *Coherent Active-Sterile Neutrino Flavor Transformation in the Early Universe*, Phys. Rev. Lett. **97**, 141301 (2006) [[astro-ph/0607403](#)].